Redox Biology 32 (2020) 101486

Contents lists available at ScienceDirect

Redox Biology

journal homepage: www.elsevier.com/locate/redox

Interaction of oxidative stress and neurotrauma in *ALDH2*$^{-/-}$ mice causes significant and persistent behavioral and pro-inflammatory effects in a tractable model of mild traumatic brain injury

Rachel C. Knopp[a,1], Sue H. Lee[a,1], Michael Hollas[a,b], Emily Nepomuceno[a], David Gonzalez[a], Kevin Tam[a], Daniyal Aamir[a], Yueting Wang[a], Emily Pierce[a], Manel BenAissa[a,b], Gregory R.J. Thatcher[a,b,*]

[a] Department of Pharmaceutical Science, College of Pharmacy, University of Illinois at Chicago, Chicago, IL, 60612, USA
[b] UICentre (Drug Discovery @ UIC), University of Illinois at Chicago, 833 S. Wood St, Chicago, IL, 60612, USA

ARTICLE INFO

Keywords:
Mild traumatic brain injury
Oxidative stress
Lipid peroxidation
Neuroinflammation
Drug discovery

ABSTRACT

Oxidative stress induced by lipid peroxidation products (LPP) accompanies aging and has been hypothesized to exacerbate the secondary cascade in traumatic brain injury (TBI). Increased oxidative stress is a contributor to loss of neural reserve that defines the ability to maintain healthy cognitive function despite the accumulation of neuropathology. *ALDH2*$^{-/-}$ mice are unable to clear aldehyde LPP by mitochondrial aldehyde dehydrogenase-2 (Aldh2) detoxification and provide a model to study mild TBI (mTBI), therapeutic interventions, and underlying mechanisms. The *ALDH2*$^{-/-}$ mouse model presents with elevated LPP-mediated protein modification, lowered levels of PSD-95, PGC1-α, and SOD-1, and mild cognitive deficits from 4 months of age. LPP scavengers are neuroprotective *in vitro* and in *ALDH2*$^{-/-}$ mice restore cognitive performance. A single-hit, closed skull mTBI failed to elicit significant effects in WT mice; however, *ALDH2*$^{-/-}$ mice showed a significant inflammatory cytokine surge in the ipsilateral hemisphere 24 h post-mTBI, and increased GFAP cleavage, a biomarker for TBI. Known neuroprotective agents, were able to reverse the effects of mTBI. This new preclinical model of mTBI, incorporating significant perturbations in behavior, inflammation, and clinically relevant biomarkers, allows mechanistic study of the interaction of LPP and neurotrauma in loss of neural reserve.

1. Introduction

Alzheimer's disease (AD), the most common form of dementia which is diagnosed in 60–80% of dementia patients, is a major cause of death in the US not amenable to therapeutic intervention with current medicines [1]. AD drug discovery strategies, largely targeting attenuation of hallmark neuropathology (amyloid-β [Aβ] and tau neurofibrillary tangles [NFT]), have failed in the clinic, despite successful proof-of-concept studies in murine preclinical models. AD and related dementia (ADRD) models need to be compatible with the realization that mixed pathology dementia is common in AD patients [2], and multiple "hits" are likely responsible for an individual's more rapid cognitive decline towards dementia [3,4]. A decline in cognitive resilience or neural reserve, linked to oxidative stress, is one likely "hit" or contributor to dementia, regardless of pathology. In this context, early to mid-life brain trauma, such as mild traumatic brain injury (mTBI) has been proposed as a "1st hit" to neural reserve that in combination with a late-life "2nd hit", such as AD pathology (Aβ and NFT) may lead to ADRD [5]. Closed head TBI has been studied in familial AD (FAD) mouse models, for example in the APP/PS1 mouse [6], wherein early Aβ accumulation and deposition represents the "1st hit".

Neural reserve, in the context of age-associated dementias, describes

* Corresponding author. University of Illinois at Chicago, 833 S. Wood St, Chicago, IL, 60612, USA.
E-mail address: thatcher@uic.edu (G.R.J. Thatcher).

[1] RCK and SHL contributed equally to this manuscript. RCK conducted *in vitro* oxidative stress experiments, assisted in data interpretation, drafted and revised the manuscript. SHL designed and directed all *in vitro* and *in vivo* experiments (LPS and mTBI), tissue preparation and execution of all inflammation, phospholipid, and histology experiments and analysis, and revised the manuscript. MH analyzed all proteomic studies and revised the manuscript. EN conducted all mTBI behavioral assays and revised the manuscript. DG, KT and DA assisted with behavioral and histology experiments. EP guided LPP measurements *in vivo* and assisted with experimental design. YTW conducted the proteomic studies. MBA assisted with experimental design and revised the manuscript. GRJT coordinated the overall project, manuscript preparation, and revision.

https://doi.org/10.1016/j.redox.2020.101486
Received 16 January 2020; Received in revised form 17 February 2020; Accepted 29 February 2020
Available online 02 March 2020

Abbreviations

Aβ	amyloid-β
AD	Alzheimer's Disease
Aldh2	aldehyde dehydrogenase 2
COX2	cyclooxygenase 2
DI	discrimination index
GFAP	glial fibrillary acidic protein
GFAP-BDP	glial fibrillary acidic protein breakdown products
HH	L-histidyl hydrazide
HNE	4-hydroxy-nonenal
IL-1β	interleukin-1 beta
KO	knock-out
LPP	lipid peroxidation products
LPS	lipopolysaccharide
MCI	mild cognitive impairment
mTBI	mild traumatic brain injury
NAC	N-acetyl cysteine
NFT	neurofibrillary tangle
NOR	novel object recognition test
ONE	2-oxononenal
TNFα	tumor necrosis factor alpha
WT	wildtype

the differing ability of individuals to preserve cognitive function despite accumulation of neuropathology that otherwise would be expected to lead inevitably to cognitive impairment [7,8]. Likely a major contributor to the loss of neural reserve is oxidative stress, which has frequently been linked to neurodegenerative disorders. Oxidative damage mediated by lipid peroxidation products (LPP) has been shown to play a significant role in the early stages and in the progression of mild cognitive impairment (MCI) [9,10], ADRD [11–15], and TBI neuropathy [12,16,17]. The LPPs, 4-hydroxynonenal (HNE), malondialdehyde (MDA), acrolein, and 4-oxo-2-nonenal (ONE) are electrophiles that covalently modify and sometimes crosslink proteins and nucleic acids [18,19]. HNE has received most attention because HNE-protein adducts have been shown to be elevated in the amygdala, hippocampus, and parahippocampal gyrus of TBI patients [17,20–22], as well as patients with MCI [10,23] and AD [24,25]. Preclinical animal models that manifest elevated brain levels of HNE-protein adducts may therefore provide novel and relevant models of the interplay of oxidative stress with attenuated neural reserve.

Amongst pathways of LPP detoxification, the enzyme action of certain glutathione-S-transferases and mitochondrial aldehyde dehydrogenase-2 (Aldh2) are recognized as primary contributors, ablating the reactive, electrophilic alkene and aldehyde groups of HNE, respectively. The *ALDH2*$^{-/-}$ mouse was developed to study Aldh2-mediated metabolism in the liver and is viable and overtly healthy [26]. This mouse was subsequently observed to display a cognitive deficit amenable to pharmacotherapeutic intervention [27,28]. More widely studied are transgenic mice bearing mutations in *ALDH2*. Aldh2*2, more commonly referred to as the "Asian allele", is a common loss-of-function mutation in *ALDH2*, proposed to contribute to AD risk in the East Asian population and to *APOE4* risk in AD, and also to risk of Parkinson's disease (PD) [29–33]. Transgenic Aldh2*2 mice were reported to develop neurodegeneration after 1 year (20% of mice) that increased to 78% of mice after 1.5 years, without significant defects in motor or sensory functions [34]. The double knockout of *ALDH1A1* and *ALDH2* has been proposed as a model for PD [35].

Various "2-hit" models have been studied wherein TBI is the 2nd hit. For example, in APP/PS1 mice, TBI worsened behavioral responses, accelerated presentation of hallmark AD pathology, and elevated neurotoxic LPPs [6]. In aged rats, TBI caused a similar phenotype, and HNE was reported to be increased one day post-injury, an effect that was sustained for one week [17]. In younger animals and those without advanced neuropathology caused by genetic mutations, mTBI generally does not produce significant effects. Chronic oxidative stress has been reported to exacerbate damage caused by TBI and to drive secondary inflammatory cascades [36,37]. LPPs, particularly HNE, are elevated following TBI, accelerating TBI-induced secondary damage [17,38]. We anticipated that mTBI in the *ALDH2*$^{-/-}$ mouse would cause a significant and observable phenotype against the background of accelerated oxidative stress. In utilizing a closed-head free weight drop model of mTBI, we characterized the impact of a single hit in the *ALDH2*$^{-/-}$ mouse model. Significant effects were observed on neuroinflammation, neuronal and synaptic plasticity markers, and cognitive function, which were not significant in WT littermates. This new model of mTBI will allow both the study of the role of LPPs in attenuated neural reserve and testing of therapeutic agents in a tractable model that does not require aged mice, nor open head or other surgery.

2. Materials and methods

All chemicals and reagents were purchased from commercial sources in the highest purity and were used as received. RIV-1061 (NMZ) was synthesized in-house according to our previous literature [39]. 4-Hydroxynonenal and 2-oxo-nonenal were purchased from Cayman Chemical (Michigan, USA). Donepezil hydrochloride, arecoline hydrobromide, memantine hydrochloride, galantamine hydrobromide, chlormethiazole hydrochloride and lipopolysaccharides (from *Escherichia coli* O111:B4) were all purchased from Sigma (Missouri, USA). All data was generated, reported and analyzed as the mean ± S.E.M. using ANOVA with Dunnett or Tukey's multi-comparison analysis using Graph-Pad Prism version 7.0.

2.1. Cell culture

Human neuroblastoma SH-SY5Y cells (ATTC CRL-2266) and CCF-STTG1 cells (ATTC CRL-1718) were cultured in DMEM/F12 (Gibco) and supplemented with 10% fetal bovine serum (Gemini Bio) and 1% penicillin-streptomycin at 37 °C in a humidified atmosphere of 5% CO_2. For cytotoxicity studies, cells were seeded at 2×10^4 cells per well in a 96-well plate in low serum media (1% fetal bovine serum). After overnight incubation, cells were administered with varying concentrations of compounds for defined periods of time. Cell viability was determined using the CellTiter 96 Aqueous One Solution Cell Proliferation Assay (MTS, Promega) and LDH release using CytoTox 96 Non-Radioactive Cytotoxicity Assay (Promega) according to the manufacturer's instructions. The experiments were performed in triplicate on at least two cell passages.

2.2. Animals

All animal care and procedures were conducted with approved institutional animal care protocols and in accordance with the NIH Guide for the Care and Use of Laboratory Animals. All animal protocols were approved by the University of Illinois at Chicago Institutional Animal Care and Use Committee (ACC#17-029). The experiments use progeny of the *ALDH2*$^{-/-}$ mice originally generated by gene targeting knockout by Kitagawa et al., [26], which were then backcrossed with C57BL/6 mice for more than 10 generations. WT littermates and knockout mice are generated from mating heterozygotes, and genotyping the progeny by PCR analysis of genomic DNA extracted from ear punches. As no sex differences were observed in any of the memory tasks, both male and female mice were combined for all studies. All treatments were via

intraperitoneal injection (i.p), unless otherwise noted. Doses of neuroprotective compounds, selected on the basis of literature examples [27,40–42], [43] were as follows: 10 mg/kg galantamine, 20 mg/kg memantine, 10 mg/kg arecoline, 10 mg/kg L-histidyl hydrazide, 1 mg/kg chlomethiazole, 1 mg/kg NMZ.

2.3. Behavioral tests

Novel Object Recognition: The NOR protocol was modified from the literature. [44] For the habituation phase, mice were allowed to explore the empty test box for 5 min, returned to home cage, and allowed to explore the empty test box again for 5 min. 24 h later, mice were subjected to the familiarization and testing phase. For the familiarization phase, two identical objects (small Lego towers) were placed in opposite corners of the test box. Mice were placed into the test box and allowed to freely explore for 10 min. For the testing phase, one original object (from the familiarization phase) and one novel object (plastic vial filled with bedding) were placed in opposite corners of the test box, maintaining location and orientation from the preceding familiarization phase. Mice were allowed to freely explore for 10 min or until the objects were explored for a total of 20 seconds. The amount of time (sec) spent exploring was recorded for both the novel object and original object to calculate the discrimination index ($DI\% = (time_{novel\ object} - time_{familiar\ object})/time_{total\ of\ exploration\ for\ both}$). Y-maze: *Spontaneous Alternation:* Mice were recorded on a Y-shaped maze and allowed to freely explore the three arms. The number of arm entries and the time spent in each arm were measured and the percentage of alternation was calculated ((%alternation = ratio of actual/possible alternations-total arm entries)*100). *Forced Alternation:* For the habituation phase, visual cues were placed on walls surrounding the Y-maze with one arm (randomized) of the Y-maze blocked. Mice were allowed to freely explore for 7 min and returned back to their home cage for 30 min. For the testing phase, all three arms of the Y-maze were opened, and mice were allowed to explore for 7 min. The latency to enter the previously blocked arm was recorded. Barnes Maze: Mice were trained through 9 trials over 3 days (3x per day) and given a probe test on the fourth day. The number of errors made and distance and time it took for mice to find the target hole were measured. Mice were tracked using a Logitech HD 1080p video system mounted overhead. Nesting: The nesting protocol was modified from *Deacon, RM.* [45] Nestlets were put into cages of individually housed mice. The next day, nests were recorded and rated on a 5-point scale ranging from 0 (no nest) to 5 points (perfect nest).

2.4. Closed head mTBI

Protocol was modified from previous literature [46]. Mice were anesthetized with isoflurane (5% flow rate) and immediately placed under the vertical 30 cm long guide tube and stabilized and positioned using a sponge cushion. A 30g weight with a rounded tip (34 × 13 mm) was dropped vertically through the tube and directed to the right sagittal plane between the eye and the ear, inducing a unilateral injury on the closed head (intact skull and scalp). Following injury, the mice were monitored for return of normal gait and no cerebral edema or seizures. Behavior tests were evaluated 1, 7, 14 and 30 days post-mTBI injury.

2.5. Tissue preparation

Mice were sacrificed using CO_2 asphyxiation, perfused with ice-cold PBS, brains extracted and split into 2 hemispheres (ipsilateral vs. contralateral), flash frozen in liquid nitrogen, and stored at −80 °C for further protein or RNA extractions. For immunohistology samples, whole brains were stored in 4% paraformaldehyde until further immunohistochemical processing. Protein Extraction for Western Blot: Hemispheres were homogenized in ice cold lysis buffer (25 mM HEPES pH 7.0, 1 mM EDTA, 1 mM EGTA, 1% Triton X-100, 0.1% SDS, protease inhibitors and phosphatase inhibitors (Roche Diagnostics)) by weight using a rotor-stator homogenizer and centrifuged at 10,000 × *g* for 10 min at 4 °C. Supernatant was collected and protein levels were measured using the BCA Protein Assay Kit (Thermo Scientific). RNA Extraction for Real Time qRT-PCR: Brains were homogenized in Trizol (Invitrogen) using a hand-held pestle homogenizer and spun at 10,000 × *g* for 10 min at 4 °C to remove cellular debris. RNA was isolated according to the manufacturer's instructions and reconstituted in 30 μL of H_2O. First strand cDNA synthesis was synthesized with 2 μg total RNA using the SuperScript III First-Strand Synthesis System for qRT-PCR (Invitrogen) according to manufacturer's instructions. Inflammation primers were acquired from Applied Biosystems. Each PCR reaction was carried out using the Taqman Gene Expression Master Mix (Applied Biosystems) on the StepOnePlus Real Time PCR system (Life Technologies). $\Delta\Delta C_T$ values for each gene were normalized to the expression level of β-actin in each sample.

2.6. Tandem mass tag (TMT) proteomics

Hippocampi and cortices from control or treated mice were homogenized in ice cold lysis buffer (RIPA with protease and phosphatase inhibitor cocktails, Roche) by weight using a benchtop bead homogenizer (Fisher). The BCA protein assay was used to measure protein content. Samples were incubated with TMT isobaric tags [47]. All samples were analyzed by LC-MS/MS. All protein identification and relative quantitation was done using Scaffold. Scaffold (version Scaffold_4.8.4, Proteome Software Inc., Portland, OR) was used to validate MS/MS based peptide and protein identifications. Peptide identifications were accepted if they could be established at greater than 84.0% probability to achieve an FDR less than 1.0% by the Scaffold Local FDR algorithm. Protein identifications were accepted if they could be established at greater than 5.0% probability to achieve an FDR less than 5.0% and contained at least 2 identified peptides.

2.7. Immunoblots

Whole brain homogenates (2 mg/mL) were incubated with 500 μM Alexa488 hydrazide (ThermoFisher) in 0.1 M phosphate buffer (pH = 5.5) for 2 h at room temperature. These proteins were then separated on a 4-12% Bis-Tris, SDS-PAGE gel (Invitrogten) with 30 μg of protein. Gels were immediately imaged using a GE Typhoon Trio imager. Western Blots: Lysates were stored at −20 °C before use. Equal amounts of protein were incubated under reducing conditions (1% β-mercaptoethanol) with 4X NuPAGE LDH sample buffer (ThermoFisher), and run on 4-12% SDS NuPage Gels (Invitrogen). Proteins were transferred to PVDF membranes using the iBLOT2, blocked in 5% non-fat milk for 1 h in room temperature, and probed with the appropriate primary antibodies overnight at 4 °C (1:500–1:2000 in blocking buffer). The following day, membranes were washed 3x with TBS-T (TBS + 0.1% Tween-20) for 5 min each and probed with an HRP-linked secondary antibody (1:1000 in blocking buffer) for 1 h in room temperature, then washed again 3x with TBS-T. Gels were visualized using SuperSignal West Femto Chemiluminescence substrate (ThermoFisher) on the Gel Doc XR + System (Biorad). Membranes were re-probed for β-actin (loading control) and stored at 4 °C until imaging. All values were normalized to expression levels of β-actin and normalized to control at 1.

2.8. Immunohistochemistry

Brains stored in 4% paraformaldehyde were subjected to a sucrose gradient (30% sucrose for the first 24 h, then 20% sucrose until slicing) and stored at 4 °C. Serial coronal brain sections (30 μm) of whole brains were cut frozen using the SM2010R sliding microtome and stored in a cryoprotection solution until ready for analysis. Slices were immunohistochemically processed using antibodies against 4-

hydroxynonenal (HNE-S: Alpha Diagnostics), GFAP (Daiko), NeuN (Santa Cruz) and counterstained with hematoxylin (Jackson Laboratories). Slides were mounted and visualized using the BZ-X700 microscope (Keyence) and further analyzed on ImageJ. From each slice, a total of 6 digital fields were analyzed. Levels of optical density were corrected to background using sections stained in the absence of the primary antibody.

3. Results

3.1. LPP-induced phenotypic effects in *ALDH2*$^{-/-}$ mice

Levels of modified LPP in whole brain lysates of WT and *ALDH2*$^{-/-}$ mice were quantified with a fluorescently tagged hydrazine probe that reacts with the free aldehyde of HNE-modified proteins. The probe revealed a significant increase in LPP modifications in the *ALDH2*$^{-/-}$ brains compared to WT at 3 and 6 months, although no obvious differences were observed between age groups (Fig. 1A; Supplemental Fig. S1A). Moreover, immunohistochemical staining verified the increase in HNE-modified proteins in both the cortex and hippocampus (Fig. 1B; Supplemental Fig. S1B). The cerebral cortex and hippocampus were isolated to identify regional differences. Staining for NeuN (a neuronal marker) revealed no significant neuronal loss in older (9-month-old) *ALDH2*$^{-/-}$ mice (Fig. 1C and 1D); however, immunoblots revealed a decrease of neuronal and synaptic plasticity markers (PSD-95 and pCREB) in both the cortex and hippocampus (Fig. 1E and F, respectively; and Supplemental Fig. S1C). PGC-1α (mitochondrial regulator) and SOD1 (mitochondrial antioxidant gene) were significantly decreased in the cortex but not the hippocampus of *ALDH2*$^{-/-}$ mice (Fig. 1G and H, respectively).

3.2. LPP-induced phenotypic effects in vitro

To mimic the effects of oxidative stress *in vitro*, neuronal cells were treated with both exogenous LPP (HNE and ONE) in the absence or addition of secondary insults. SH-SY5Y cells were treated with the LPPs, HNE and ONE, and assessed for cell viability (MTS assay) to understand the dose-dependent phenotypic effects of LPPs *in vitro*. Treatment with HNE (1-10 μM) caused a concentration-dependent loss of cell viability measured at 24 h. However, increasing HNE concentration from 10 μM to 50 μM did not significantly increase the observed ~45% cell death, consistent with previous literature (Fig. 2A) [48]. Since the plateau effect (at ≥ 10 μM HNE) indicates induction of cell stress response pathways that protect against higher HNE concentrations, cells were pre-incubated with selective inhibitors (10 μM) of kinase pathways that might mediate stress response (PD980589 for MAPK/ERK, GDC0994 for CAMK, KN93 for JNK, honokiol for p38MAPK). Cells pretreated with KN-93 and honokiol showed significantly exacerbated cell death at 10 μM, but blocking these stress response pathways did not overcome the plateau effect (Supplemental Fig. S2A).

Unsurprisingly, in part because of its greater reactivity, ONE (0.1–25 μM) was more cytotoxic, producing ~15% cell death at 0.1 μM and dose-dependent neurotoxicity up to 25 μM (~75% cell death). All observations on cell viability using MTS were corroborated using secreted LDH as a marker of cell death (Fig. 2B).

Oxidative stress is hypothesized to play a driving role in the secondary cascade of single and multiple hit mTBI [49]. To mimic the effects of a "2nd hit" *in vitro*, cells were treated with exogenous HNE (1st hit) and various insults (2nd hit) to test if an underlying level of oxidative stress, caused by HNE, would exacerbate the neuronal loss subsequent to a second insult (Supplemental Fig. S2C). SH-SY5Y cells were pretreated for 2 h with 5 or 10 μM HNE then treated with: 1) H_2O_2 and ROS generating iron ascorbate (Fe-Asc); or 2) a bacterial toxin (lipopolysaccharide; LPS). Cell viability was quantified and normalized to HNE-treated cells. Exacerbated cell death was observed with all three insults (Fig. 2C): Fe-Asc: control = 98.2 ± 6.2%, 5 μM HNE = 77.9 ± 1.3%, 10 μM HNE = 76.1 ± 0.9%; H_2O_2: control = 68.6 ± 0.2%, 5 μM HNE = 62.6 ± 2.2%, 10 μM

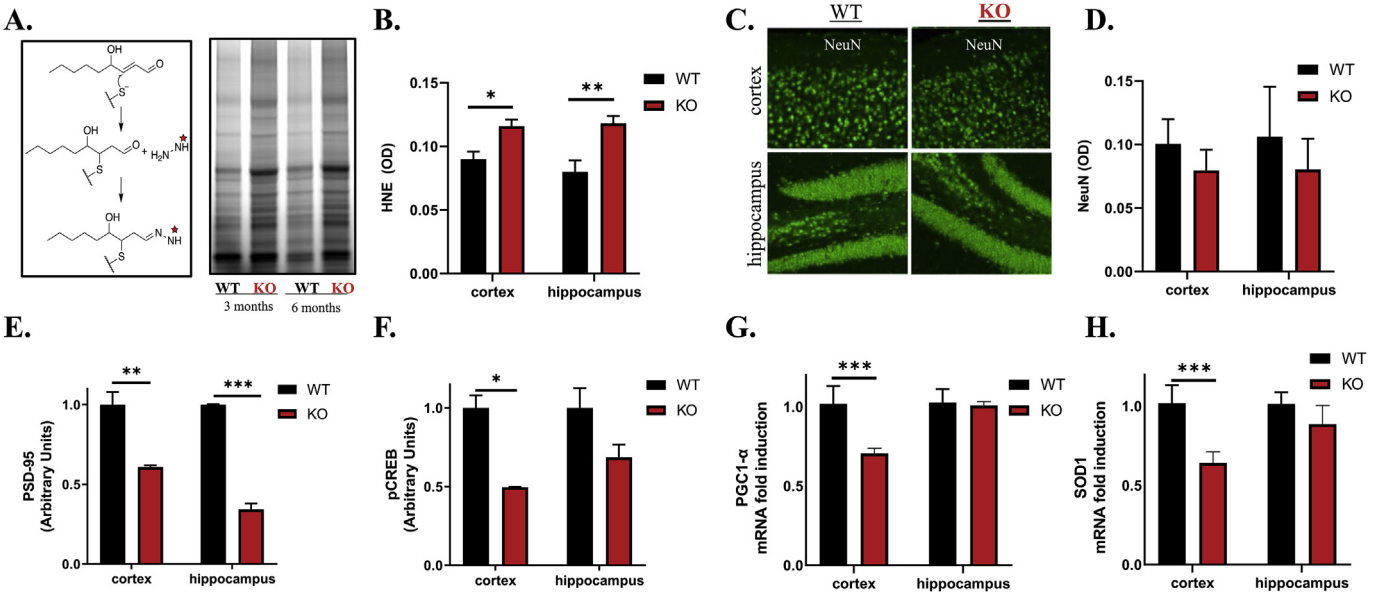

Fig. 1. *ALDH2*$^{-/-}$- mice exhibit elevated HNE adduction and diminished markers of synaptic and mitochondrial function without appreciable neuronal loss. (**A**) Schematic representation of the hydrazine reacting with the free aldehyde of HNE-modified proteins and corresponding immunoblots of whole brain lysates of 3 or 6 month old *ALDH2*$^{-/-}$ mice or WT littermates incubated with the hydrazine. (**B**) Quantitative analysis of 6 month old WT and *ALDH2*$^{-/-}$ cortex and hippocampus lysates probed with a HNE antibody measured by optical density. (**C** and **D**) Representative immunofluorescent images of 9 month old WT and *ALDH2*$^{-/-}$ cortex and hippocampus slices stained for NeuN, and quantitative analysis in optical density units. Optical density was measured for the entire image displayed. (**E** and **F**) Quantitative immunoblot analysis of 14 month old cortex and hippocampal homogenates of PSD-95 (95 kDa, E) and pCREB (35 kDa, F). (**G** and **H**) qRT-PCR analysis of PGC-1α (**G**) and SOD1 (**H**) gene expression in 14 month old cortex and hippocampus homogenates. All genes and proteins were normalized to the housekeeping gene, β-actin. Equal protein amounts were loaded in all lanes of immunoblots. Data represent mean ± S.E.M analyzed by one-way ANOVA with Dunnett's or Tukey's multi-comparison analysis from n = 8–10 mice/genotype/age (*P < 0.05, **P < 0.001, ***P < 0.001).

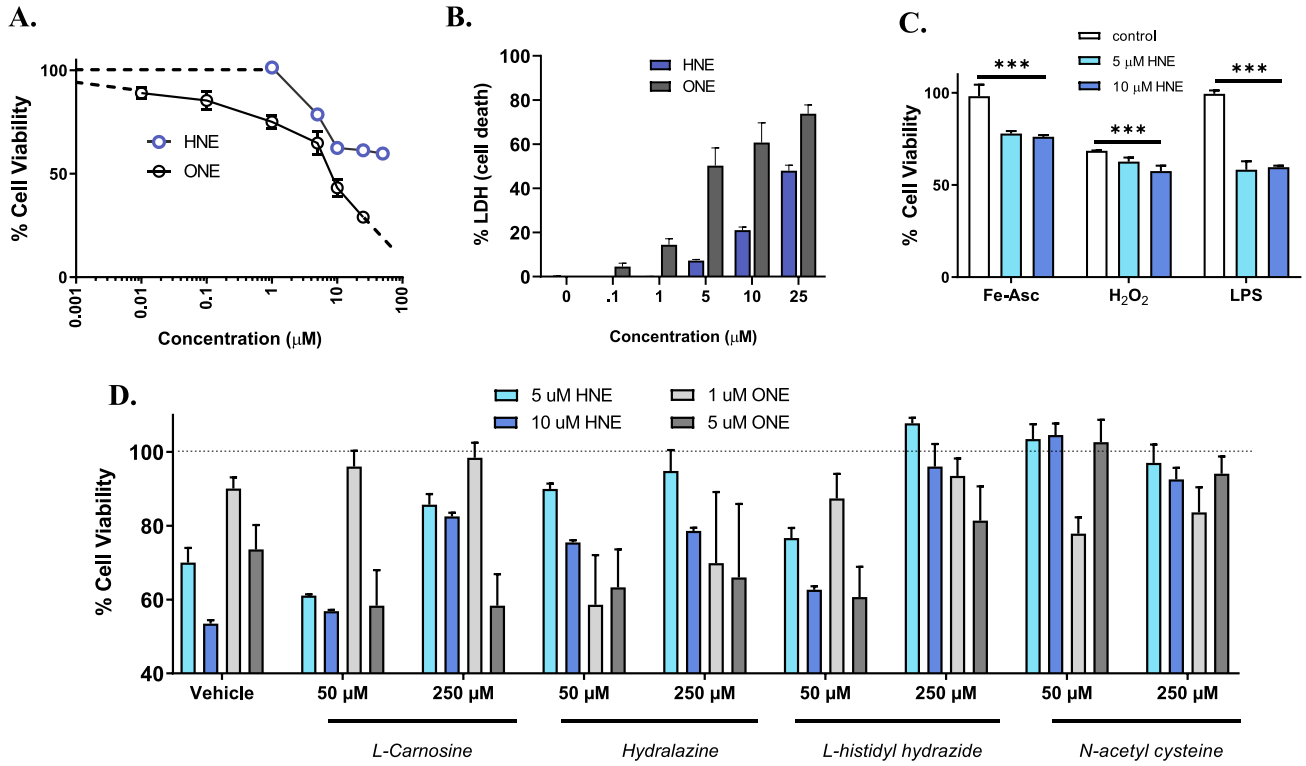

Fig. 2. Oxidative stress induces neuronal loss and exacerbates stress response *in vitro*. (**A** and **B**) Cell viability of SH-SY5Y cells incubated with either HNE (0-50 μM) or ONE (0-25 μM) for 24 h with cell viability quantified by MTS **(A)** and LDH (**B**). (**C**) Cell viability of SH-SY5Y cells treated with either 5 or 10 μM HNE for 2 h and insulted with second neurotoxin for 24 h with cell viability normalized to HNE-treated cells and quantified by MTS. Concentrations for the neurotoxins were as follows: 50 μM iron ascorbate (Fe-Asc), 50 μM hydrogen peroxide (H2O2) and 1 μg/mL lipopolysaccharide (LPS). (**D**) Cell viability of SH-SY5Y cells co-treated with well-studied scavengers (50 μM and 250 μM) and either HNE (5 μM and 10 μM) or ONE (1 μM and 5 μM) for 24 h with cell viability quantified by MTS. Data represent mean ± S.E.M. analyzed by one-way ANOVA with Dunnett's or Tukey's multi-comparison analysis from three cell passages (n = 6/passage, *P < 0.05, **P < 0.01, ***P < 0.001).

HNE = 57.6 ± 2.9%; LPS: control = 99.4 ± 1.9%, 5 μM HNE = 58.2 ± 4.6%, 10 μM HNE = 59.6 ± 0.8%). The primary reaction of both H_2O_2 and HNE with proteins is with cysteine residues. Unsurprisingly, since both H_2O_2 and HNE compete for reactive cysteines, the effect of the combination is muted. Moreover, Nrf2 levels significantly increased with the "2nd hit" (Supplemental Fig. S2B). This trend was also observed on treatment of SH-SY5Y 3D "neurospheres" (Supplemental Fig. S3).

3.3. LPP scavenging agents attenuate the LPP-induced phenotype in vitro

Scavenging agents were compared to determine the relative potential to alleviate the impact of increased LPPs in cell cultures. The agents selected, and their concentrations, were well characterized in the literature [50–52]. Additional control experiments of cells treated with the scavengers alone had no effect on cell viability. SH-SY5Y cells were co-treated with both scavengers (50 μM and 250 μM) and LPPs (HNE: 5 μM and 10 μM; ONE: 1 μM and 5 μM), and cell viability was measured at 24 h via MTS and LDH. N-acetyl cysteine (NAC) displayed the highest level of neuroprotection at 50 μM (Fig. 2D). All scavengers, including hydralazine and L-carnosine, showed some neuroprotection. At 250 μM, L-histidyl hydrazide (HH) and NAC were equivalent and superior to other scavengers in their neuroprotective actions. To test an LPP scavenger *in vivo*, we selected HH, since NAC has mechanisms beyond scavenging LPP, including as a scavenger of reactive oxygen species, and a precursor of L-cysteine and glutathione [53[93]].

3.4. LPP-induced cognitive deficits in $ALDH2^{-/-}$ mice reversed by LPP scavenging and pro-cognitive agents

To establish the effect of LPP on behavior, $ALDH2^{-/-}$ mice and WT littermates were studied in various cognitive tasks at 9 months of age. No significant differences were observed between $ALDH2^{-/-}$ mice and WT littermates in body weight or in nesting behavior (Supplemental Figs. S4A and B). The behavioral studies consisted of four tests specifically chosen to evaluate various aspects of cognitive impairment: Y-maze forced alternation task, Y-maze spontaneous alternation task, Barnes maze, and novel object recognition test (NOR). The well-characterized Y-maze forced alternation task tests working memory and disposition to explore new environments, measuring the latency to enter a previously blocked arm [57]. $ALDH2^{-/-}$ mice had significantly longer latency to enter the novel arm (WT 8.7 ± 2.4 s, $ALDH2^{-/-}$ 69.1 ± 30.1 s, Fig. 3A, Supplemental Sig. S4C and S4D). In the Y-Maze spontaneous alternation task, testing working memory and exploratory behavior, 50% represents an unbiased exploration of the choices available [57]. $ALDH2^{-/-}$ mice performance was significantly worse than WT: $ALDH2^{-/-}$ 27.9 ± 4.6, WT 52.2 ± 315.69 (Fig. 3B). The Barnes Maze task, a dry land-adapted version of the Morris Water Maze, tests hippocampal spatial learning and memory [58,59]. In this test, mice are confined to a training platform with multiple holes, one of which is an escape route surrounded by visual cues. $ALDH2^{-/-}$ mice exhibited no deficit in short-term memory as measured by a decrease in errors each day in the 3-day training period compared to their WT littermates (Supplemental Figs. S4C and D). During the final probe test, WT mice found the target more quickly and spent more time in the target quadrant than the $ALDH2^{-/-}$ mice (Fig. 3C).

The NOR task is a widely used behavioral tests to assess recognition

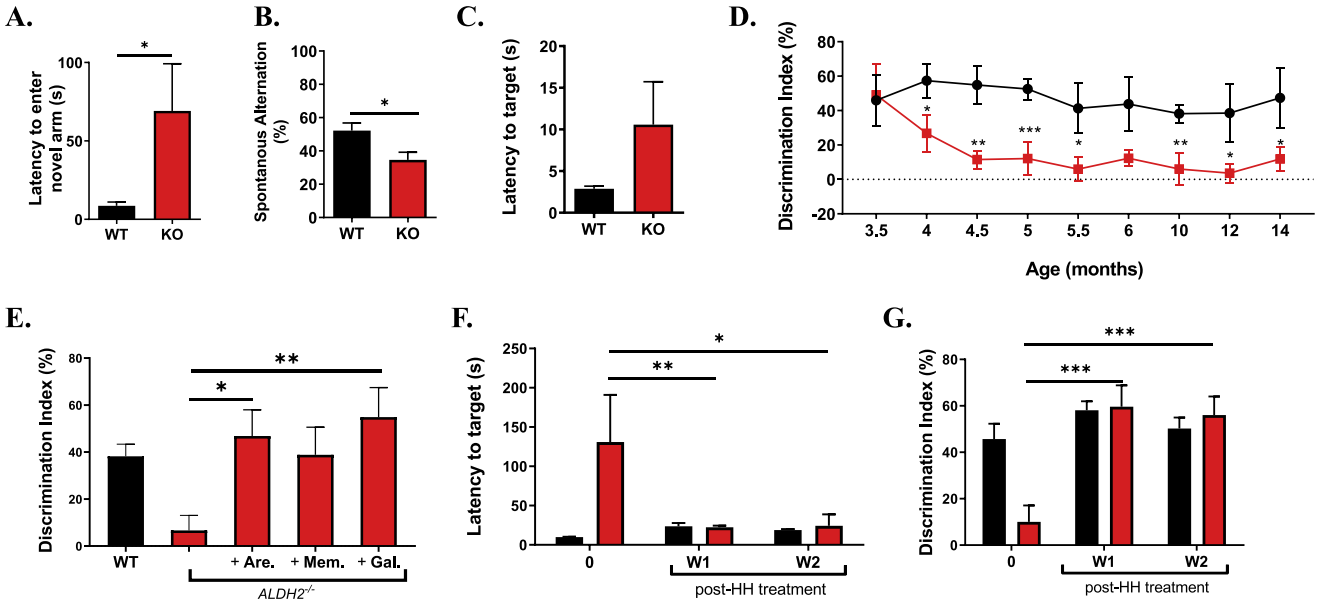

Fig. 3. *ALDH2*$^{-/-}$ mice have a mild phenotype and exhibit mild cognitive impairment that is reversed by pro-cognitive agents. (**A** and **B**) Quantitative analysis of the performance of WT and *ALDH2*$^{-/-}$ mice in the Y-maze forced alternation (**A**) task which measures latency to enter a previously locked arm and the spontaneous alternation (**B**) task which measures the exploration of the arms available. (**C**) Quantitative analysis of the performance of WT and *ALDH2*$^{-/-}$ mice in the Barnes maze, which measures ability of mice to find a hidden target.(**D**) Quantitative analysis of the performance of WT and *ALDH2*$^{-/-}$ mice in the novel recognition (NOR) test, which measures recognition memory, from 3.5 through 10 months. (**E**). Cognitive performance of *ALDH2*$^{-/-}$ mice treated with 10 mg/kg Arecoline (Are), 20 mg/kg Memantine (Mem) or 10 mg/kg Galantamine (Gal) via i.p. 20 min prior to the familiarization phase in the NOR test, and tested for their DI % in the testing phase. (**F** and **G**) Quantitative analysis of the performance of 14 month old WT and *ALDH2*$^{-/-}$ mice in the Y-maze (**F**) and NOR (**G**) with daily treatment of 10 mg/kg i.p. L-histidyl hydrazide (HH). Pre-testing (0) was measured prior to beginning treatment. Unless otherwise indicated, all behavior studies were performed on 9 month old mice. Data represent mean ± S.E.M analyzed by one-way ANOVA with Dunnett's or Tukey's multi-comparison analysis from (n = 6–8 mice/group). *P < 0.05, **P < 0.01, ***P < 0.001.

memory [44]. At 3.5 months old, WT and *ALDH2*$^{-/-}$ mice show no significant difference in discrimination index (DI%, Fig. 3D). However, *ALDH2*$^{-/-}$ mice show a significant and sustained decrease in DI% beginning at 4 months (WT DI% 57.4 ± 9.8, *ALDH2*$^{-/-}$ DI% 26.8 ± 10.8, $p < 0.05$). The cognitive deficit in NOR was measured longitudinally until 14 months (WT DI% 47.4 ± 17.4, *ALDH2*$^{-/-}$ DI% 11.9 ± 7.2, $p < 0.05$). The *ALDH2*$^{-/-}$ mouse model can be classified as one of accelerated cognitive decline; although, no further significant decline was seen from 4 to 14 months, in agreement with previous observations [28]. Moreover, the cognitive impairment observed in the behavioral tests are compatible with the decrease in hippocampal synaptic markers (Fig. 1E and F).

To further validate and understand the memory deficits seen in the *ALDH2*$^{-/-}$ mice, known pro-cognitive agents were administered to see if the deficits were reversible. Arecoline (acetylcholine receptor agonist), memantine (NMDA receptor antagonist), and galantamine (acetylcholinesterase inhibitor) were selected as anti-amnestic agents or approved AD therapies [43,60,61]. *ALDH2*$^{-/-}$ mice (9-month-old) were treated with procognitive agents 20 min prior to training in NOR. Testing the following day showed significant effects for arecoline and galantamine (46.9% ± 11.1 and 54.9% ± 12.6 respectively), whereas the effect of memantine did not reach significance (Fig. 3E).

To test an LPP scavenger in the *ALDH2*$^{-/-}$ model, HH was administered to 14-month-old *ALDH2*$^{-/-}$ mice and WT littermates for 2 weeks (10 mg/kg/day i.p.), with weekly behavioral tests in NOR and the Y-maze forced alternation tasks, compared to pre-treatment testing. After only 1 week of HH treatment, cognitive deficits in the *ALDH2*$^{-/-}$ mice were reversed in both the Y-maze (Pretest: 130.9 ± 60.0, Post 1 week: 24.0 ± 2.0, $p < 0.01$, Post 2 week: 21.3 ± 8.9, $p < 0.05$, Fig. 3F) and NOR (Pretest: 10 ± 3.8, Post 1 week: 59.6 ± 9.2, $p < 0.001$, Post 2 weeks: 56.0 ± 8.0, $p < 0.001$, Fig. 3G) tests. This effect was sustained throughout 2 weeks of treatment, with no significant effect observed in the WT littermates.

3.5. TMT proteomics identified only small changes in protein expression in *ALDH2*$^{-/-}$ mice

Cortices of older *ALDH2*$^{-/-}$ mice were extracted to understand how the proteome is modulated by the genetic disturbance using unbiased tandem mass tag (TMT) differential proteomics. A total of 4903 proteins in 4493 clusters were identified in the cortex of the WT and *ALDH2*$^{-/-}$ mice. Intriguingly, only four were found to be significantly varied (Supplemental Fig. S5A). Unsurprisingly, Aldh2 was found to be "downregulated", while Tmem2, a regulator of Vascular Endothelial Growth Factor (VEGF) was found to be upregulated (Fig. 4C) [62]. Since HH rapidly restored normal cognitive function, it was of interest to test for proteins differentially regulated by HH in *ALDH2*$^{-/-}$ mice versus HH treated controls. When *ALDH2*$^{-/-}$ mice treated with HH were compared to WT treated with HH, 11 proteins were found differentially expressed (obviously including Aldh2, Fig. 4A and B). Nedd, a ubiquitin-like protein, and Wdfy1, a protein involved in inflammatory processes, were found upregulated in *ALDH2*$^{-/-}$ mice. Moreover, collagen proteins Col1a1 and Col1a2 were downregulated. However, when comparing the HH-treated versus vehicle-treated *ALDH2*$^{-/-}$ mice only one protein, Fgb, was observed to be differentially expressed (Supplemental Fig. S5B). Overall, only 16 proteins were significantly altered (Fig. 4B and 4C, p < 0.04). Although further follow up studies are indicated, the TMT-proteomic analysis did not demonstrate widespread changes in protein expression in the brains of *ALDH2*$^{-/-}$ mice, which is compatible with the MCI that responds rapidly to anti-amnestic and LPP scavenging agents. It might be speculated that changes are occurring at the level of post-translational modification. While there was an observable decrease in PSD-95 in immunoblots, this protein was not detected in the proteomic data.

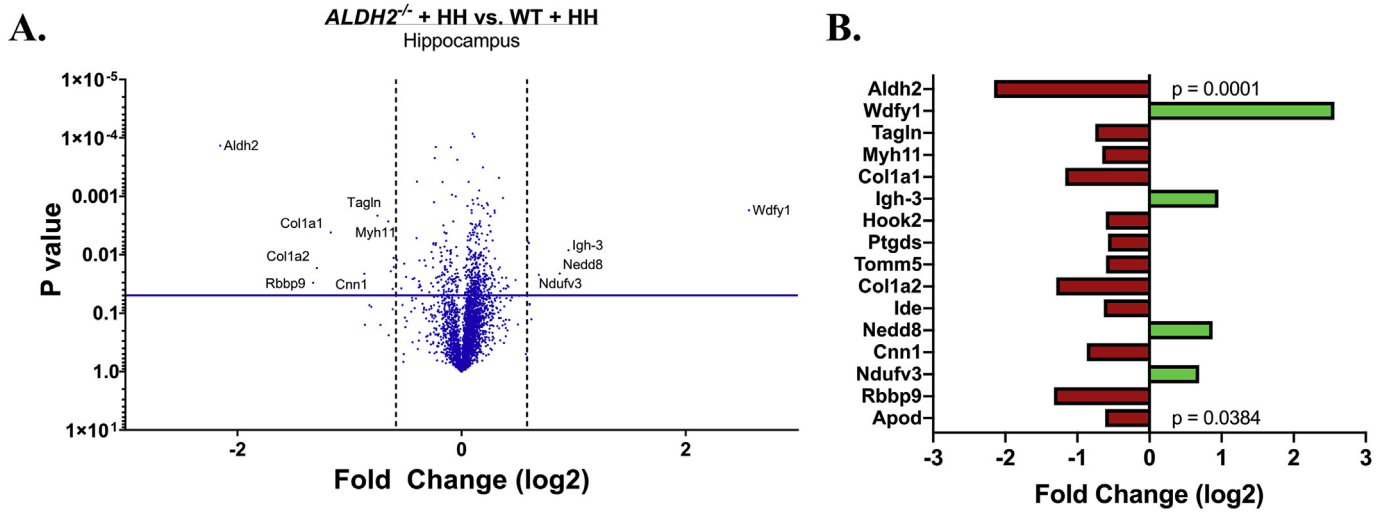

C.

Gene	Protein	Function	log2 fold
***ALDH2-/-* vs. WT cortical tissues**			
Wdfy1	WD repeat and FYV E domain-containing protein 1	Promotes activation of transcription factors IRF3 and NF-kappa-B, as well as production of IFN-beta and inflammatory cytokines	+2.6
Igh-3	Ig gamma-2B chain C region	Phagocytosis, positive e regulation of immune response	+0.95
Nedd8	Neddylin	Ubiquitin-like protein	+0.88
Ndufv3	NADH dehydrogenase	Mitochondrial ATP synthesis coupled electron transport	+0.69
Tagln	Transgelin	Actin cross-linking/gelling protein	-0.77
Myh11	Myosin-11	Nucleotide Binding & Muscle Contraction	-0.65
Col1a1	Collagen alpha-1(I) chain	Member of group I collagen (fibrillar forming collagen)	-1.17
Col1a2	Collagen alpha-2(I) chain	Member of group I collagen (fibrillar forming collagen)	-1.29
Cnn1	Calponin-1	Regulation and modulation of smooth muscle contraction	-0.87
Rbbp9	Putative hydrolase RBBP9	Serine hydrolase with unknown substrates	-1.3
***ALDH2-/-* + HH vs. WT + HH hippocampal tissues (see Supplemental for volcano plot)**			
Tmem2	Cell Migration Inducting Hyaluronidase 2	Cell surface hyaluronidase, regulates hyaluronic acid to promote normal VEGF signaling	+2.6
Clic6	Chloride intracellular channel protein 6	Regulates chloride ion transport	-1.0
***ALDH2-/-* + HH vs. *ALDH2-/-* hippocampal tissues (see Supplemental for volcano plot)**			
Fgb	Fibrinogen beta chain (Fgb)	Cell adhesion, blood coagulation	-0.81

Fig. 4. TMT protein analysis reveals subtle changes in *ALDH2*$^{-/-}$ mice. (**A**) Volcano plot comparing results of TMT proteomics from hippocampi of WT and *ALDH2*$^{-/-}$ mice treated daily with 10 mg/kg HH i.p for 2 weeks. (**B**) Bar chart showing fold change (log2) for differentially expressed proteins with significance decreasing from top to bottom. (**C**) Table describing the function of all proteins differentially expressed. Volcano plots: vertical line shows .05 P-value, while horizontal line depicts 1.5 fold change. All studies were performed on 14 month old mice.

3.6. An acute "2nd hit" exacerbates LPP-mediated pro-inflammatory cytokine surge and neuronal loss

We next studied the effect, *in vitro* and *in vivo,* of elevated LPPs on response to inflammatory insults as a "2nd hit". CCF-STTG1 cells, an astrocytoma cell line modeling astrocytes, were pretreated with 5 μM or 10 μM HNE and then treated with TNFα or LPS, 1 ng/mL or 1 μg/mL, respectively. These conditions were optimized to avoid excessive cell death (data not shown). The pro-inflammatory cytokines TNFα and IL-1β, and COX2, are key mediators of secondary injury and were used as markers to study exacerbation of LPS-induced inflammation. HNE pretreatment significantly amplified both COX2 and IL-1β mRNA expression levels in both the LPS and TNFα treated cells (Fig. 5A and B, respectively). TNFα levels, however, remained unchanged with increasing levels of HNE, which is compatible with reports suggesting exogenous HNE suppresses TNFα production through inhibition of the NF-κB transcription factor which is responsible for gene regulation during immune response [63,64].

To extend these observations *in vivo*, a pilot study was completed to determine the optimal dose for LPS treatment. Young WT and *ALDH2*$^{-/-}$ mice (3 months old) were treated with LPS at either 2 mg/kg or 4 mg/kg for 4 h before sacrifice and extraction of brain mRNA to measure inflammatory cytokine expression levels. *ALDH2*$^{-/-}$ mice treated at the 4 mg/kg dose exhibited a significant increase in TNFα (53.9 vs 25.7) and IL-1β (58.6 vs 22.7) mRNA levels compared to WT (Fig. 5C and Supplemental Figs. S6A and B). Effects on COX2 were not significant. Measurement of inflammatory markers in the plasma showed a significant increase in levels of IL-1β (Fig. 5D). Immunohistochemical staining for GFAP (glial fibrillary acidic protein) confirmed the enhanced inflammatory response in *ALDH2*$^{-/-}$ mice, showing a significant increase in activated astrocytes in the cortex (Fig. 5E, G). Moreover, neuronal density was unchanged in the hippocampus but significantly decreased in the cortex (Fig. 5F, H). These observations show that increased basal levels of oxidative stress prime the brain for amplified pro-inflammatory responses, which is compatible with literature observations [65].

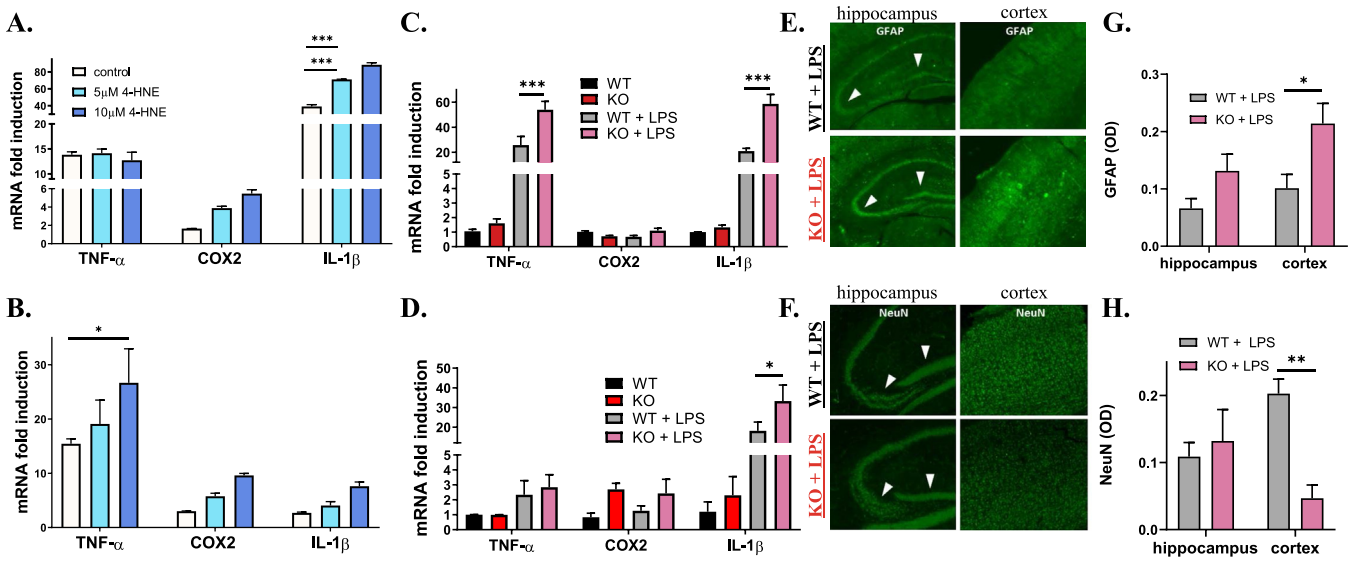

Fig. 5. Exacerbated inflammation induced by LPS *in vitro* and *in vivo* in *ALDH2*$^{-/-}$ mice. (**A** and **B**) qRT-PCR analysis of TNF-α, COX2 and IL-1β gene expression from CCF-STTG1 cells pre-treated with 5 or 10 μM 4-HNE for 2 h, followed by 1 μg/mL LPS (**A**) or 1 ng/mL TNF-α (**B**) for 24 h. (**C** and **D**) qRT-PCR analysis of TNF-α, COX2 and IL-1β gene expression from the whole brain (**C**) and plasma (**D**) of 9-month-old WT and *ALDH2*$^{-/-}$ mice with 4 h treatment of 4 mg/kg LPS or vehicle. (**E-H**) Representative immunofluorescent images of brain slices from WT and *ALDH2*$^{-/-}$ mice with 4 h treatment of 4 mg/kg LPS stained for GFAP (**E**) and NeuN (**F**) and respective quantitative analysis (**G** and **H**) in optical density units. All samples were normalized to the housekeeping gene, β-actin. Optical density was measured for the entire image displayed. Data represent mean ± S.E.M analyzed by one-way ANOVA with Dunnett's or Tukey's multi-comparison analysis from (n = 3–6): *P < 0.05, ***P < 0.001.

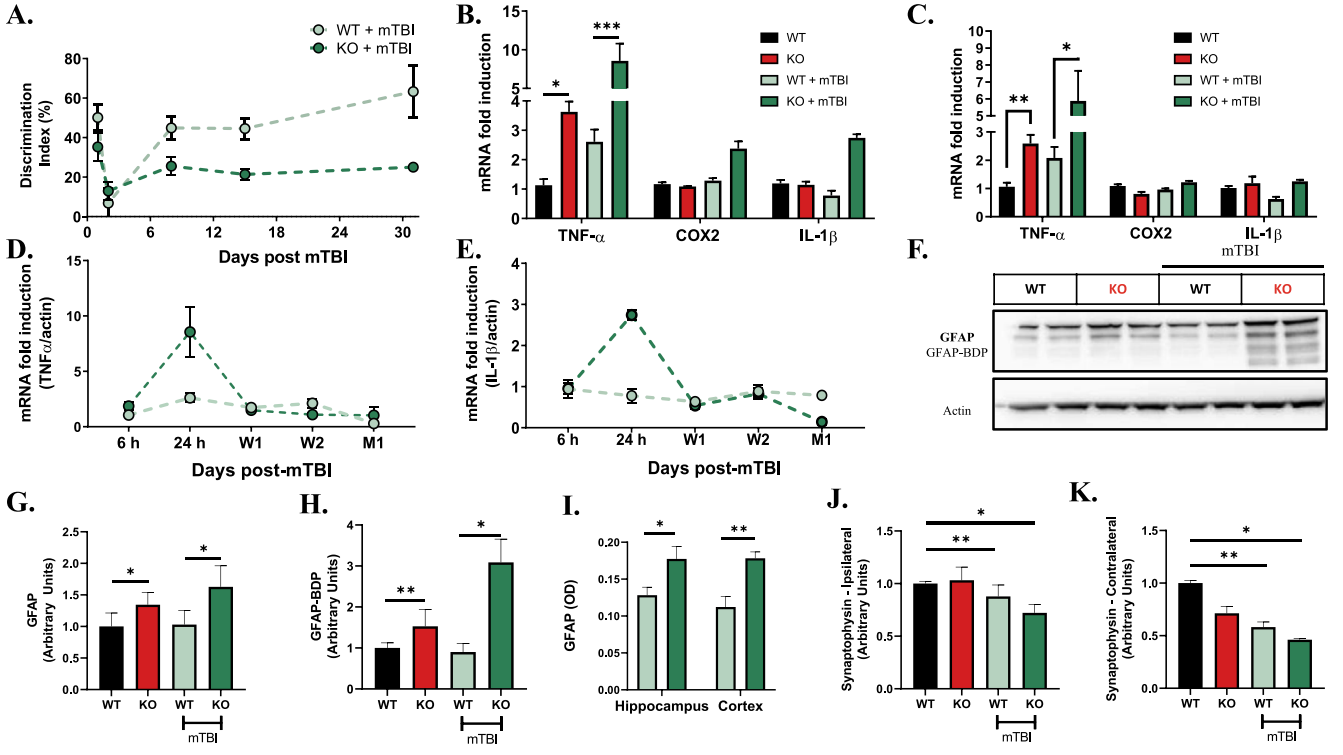

Fig. 6. mTBI induces exacerbated acute and chronic neuroinflammation and sustained cognitive deficits in the *Aldh2*$^{-/-}$ mice. (**A**) Quantitative analysis of the performance of WT and *ALDH2*$^{-/-}$ mice with mTBI or null controls in NOR for 1, 7, 14 and 30 days post-mTBI injury. (**B** and **C**) qRT-PCR analysis of TNF-α, COX2 and IL-1β gene expression in the ipsilateral (**B**) and contralateral (**C**) hemispheres of WT and *ALDH2*$^{-/-}$ mice 24 h post-mTBI and null mouse controls. (**D** and **E**). qRT-PCR analysis of TNF-α (**D**) and IL-1β (**E**) of WT and *ALDH2*$^{-/-}$ mice 6 h, 24 h, 1 week (W1), 2 weeks (W2) and 1 month (M1) post-mTBI and null mouse controls. (**F–H**) Representative immunoblot of WT and *ALDH2*$^{-/-}$ mice 24 h post-mTBI and null controls probed with GFAP Ab (**F**) with quantitative analysis of GFAP (50 kDa, **G**) and GFAP-mediated breakdown products (35–45 kDa, GFAP-BDP, **H**). (**I**) Quantitative analysis of brain slices of WT and *ALDH2*$^{-/-}$ mice 24 h post-mTBI probed with GFAP Ab in optical density units. (**J** and **K**) Quantitative analysis of immunoblots from the ipsilateral (**J**) and contralateral (**K**) hemispheres of WT and *ALDH2*$^{-/-}$ mice 24 h post-mTBI and null controls probed with synaptophysin Ab (42 kDa). All samples were normalized to the housekeeping gene, β-actin. Data represent mean ± S.E.M analyzed by one-way ANOVA with Dunnett's or Tukey's multi-comparison analysis from (n = 6) *P < 0.05, **P < 0.01, ***P < 0.001.

3.7. The effects of closed head mTBI are amplified by LPP in $ALDH2^{-/-}$ mice

Oxidative stress is hypothesized to play a driving role in the secondary cascade of effects following mTBI [49]. We utilized a closed-head weight drop insult to characterize the effects of underlying LPP in exacerbating secondary injury in mTBI. A 30 g bullet was dropped down an 80 cm long tube and directed towards the right hemisphere between the ear and the eye. The skull was intact and the head was stabilized in a sponge cradle. This model is non-stereotaxic, reflecting the heterogeneity observed in human TBI populations. No gross pathological changes in infarct damage or contusion were seen in mice that were included in data analysis. We studied mice at 2.5–3 months of age, because $ALDH2^{-/-}$ mice at this age do not show a significant deficit in spatial and exploratory behavior. Both WT and $ALDH2^{-/-}$ mice exhibited a sharp decline in NOR behavior (DI%) one day post-mTBI (Fig. 6A). WT mice recovered baseline NOR performance at one week post-injury; however, $ALDH2^{-/-}$ mice failed to improve cognitive performance. The cognitive deficit in NOR was sustained up to 1 month post-injury, which is the age at which these mice, in the absence of mTBI, begin to show a deficit in the NOR task.

Brain tissues were analyzed for changes in pro-inflammatory cytokine expression. In $ALDH2^{-/-}$ mice, pro-inflammatory cytokines were increased 24 h post-mTBI in the ipsilateral hemisphere, with changes in TNFα reaching significance (8.7-fold increase, Fig. 6B). No changes in inflammatory markers in WT mice induced by mTBI reached significance. In the contralateral hemisphere, compensating effects were observed with TNFα levels significantly increased (5.8-fold increase), while COX2 and IL-1β remained unchanged (Fig. 6C). Again, the inflammatory response of WT mice after mTBI was not significant. As inflammatory responses may be highly dynamic, TNFα, COX2 and IL-1β mRNA expression levels in the ipsilateral hemisphere were monitored over time (Fig. 6D and E; Supplemental Fig. S7A). The increased levels of TNFα and IL-1β seen in $ALDH2^{-/-}$ mice one day post-mTBI returned to baseline after 1 week. These observations show that elevated LPP and increased basal oxidative stress amplify the effects of mTBI leading to diminished cognitive function and elevated pro-inflammatory cytokines.

GFAP, a biomarker for activated astrocytes, has recently been proposed as an acute diagnostic biomarker for TBI [66–68]. Moreover, GFAP breakdown products (GFAP-BDP), generated primarily by proteolytic degradation mediated by overactivation of calpains, are observed following brain injury, and provide a potential secondary biomarker for TBI [69]. Thus, levels of GFAP and GFAP-BDP were measured by immunoblot and quantified (Fig. 6F–H; Supplemental Fig. S7B). Levels of GFAP and GFAP-BDP are significantly higher in $ALDH2^{-/-}$ relative to WT mice, compatible with observations on the interaction of oxidative stress with astrocytes and glial cell function [70]. After mTBI, levels of GFAP-BDP are significantly and dramatically increased in $ALDH2^{-/-}$ mice. Immunohistochemical staining confirmed significantly enhanced levels of GFAP in both the cortex and hippocampus of $ALDH2^{-/-}$ mice post-injury (Fig. 6I). These findings further demonstrate that increased levels of LPP and enhanced basal oxidative stress exacerbate inflammation and astrocyte activation after single hit mTBI.

PSD-95, the major scaffolding protein at excitatory synapses, and synaptophysin, a presynaptic vesicle marker, were analyzed to determine changes in synaptic markers induced by mTBI. Lower levels of PSD-95 and synaptophysin were observed in the $ALDH2^{-/-}$ versus WT brain tissues, showing impairment of neuronal synapses caused by LPP (Supplemental Fig. S8). However, post-injury there was no significant change of PSD-95 levels in either hemisphere, which is consistent with observations on PSD-95 levels one day post-injury with mTBI or moderate TBI [71,72]. Moreover, synaptophysin was significantly decreased in both hemispheres in the WT brain post-injury, an effect which was observed and not exacerbated in the $ALDH2^{-/-}$ mice (Fig. 6J and K). This suggests that any aggravation of synaptic pathology, one day post-injury, induced by elevated LPP, does not reach significance.

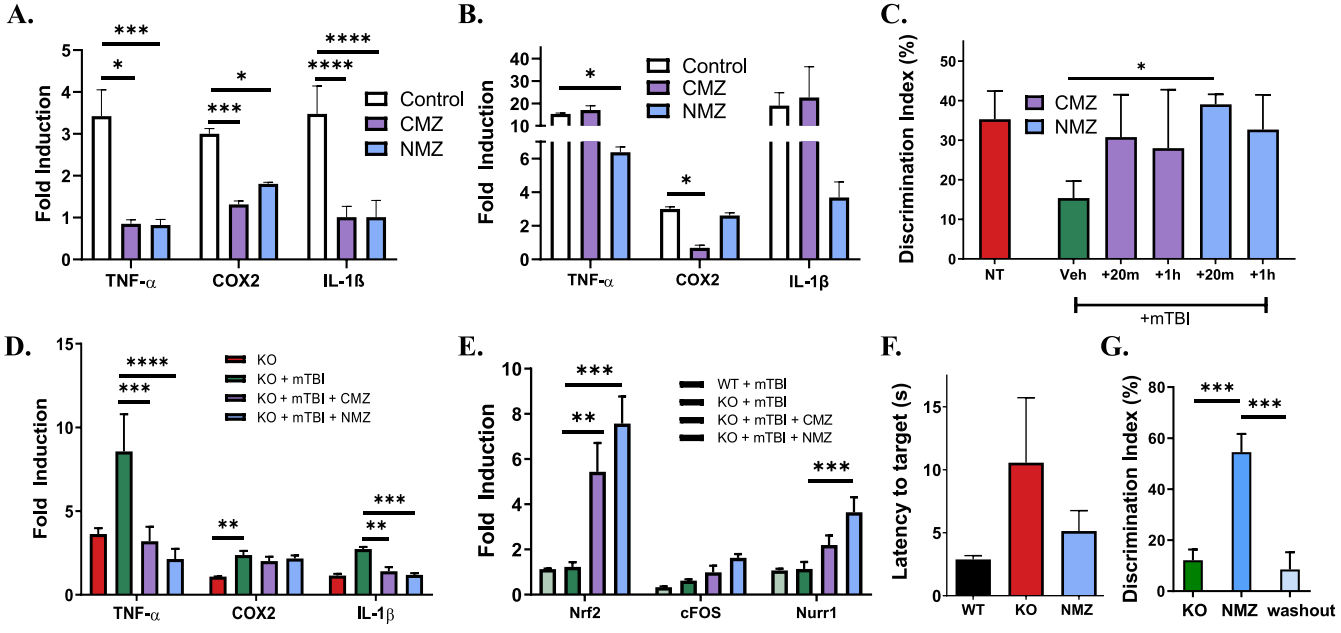

Fig. 7. CMZ and NMZ attenuate pro-inflammatory response and cognitive loss. (**A** and **B**). qRT-PCR analysis of TNF-α, COX2 and IL-1β gene expression from CCF-STTG1 cells pre-treated with 50 μM CMZ or NMZ for 24 h, followed by 1 μg/mL LPS (**A**) or 1 ng/mL TNF-α (**B**) for 24 h. (**C**) Quantitative analysis of the performance of WT and $ALDH2^{-/-}$ mice 24h post-mTBI or null controls in NOR when treated with 1 mg/kg (i.p.) CMZ, NMZ or vehicle 20 min or 1h post-mTBI. (**D** and **E**) qRT-PCR analysis of inflammatory (TNF-α, COX2 and IL-1β, **D**) or CRE IEG (Nrf2, cFOS and Nurr1, **E**) gene expression of ipsilateral hemispheres from $ALDH2^{-/-}$ mice 24h post-mTBI or null control treated 20 min post-injury. (**F** and **G**) Quantitative analysis of the performance of 9 month old $ALDH2^{-/-}$ mice in Barnes maze (**F**) or NOR (**G**) treated with single dose 1 mg/kg NMZ 20 min prior to the testing phase. The washout experiment was performed 3 days after initial treatment. All samples were normalized to the housekeeping gene, β-actin. Data represent mean ± S.E.M analyzed by one-way ANOVA with Dunnett's or Tukey's multi-comparison analysis from (n = 4–6): *P < 0.05, **P < 0.01, ***P < 0.001, ****P < 0.0001.

Intriguingly, after 1 week, levels of PSD-95 and GFAP sharply increased while synaptophysin decreased in both hemispheres (Supplemental Fig. S9). Levels of all proteins were similarly increased or decreased in the WT versus *ALDH2*$^{-/-}$ hemispheres, indicating LPP acutely exacerbates mTBI damage.

3.8. Using the *ALDH2*$^{-/-}$ mouse mTBl model to test anti-neuroinflammatory agents

Chlomethiazole (CMZ) is a drug with known neuroprotective and anti-inflammatory properties that completed clinical trials for stroke and spinal cord injury [73], whereas RIV-5061 (NMZ) has demonstrated these same attributes, in addition to pro-cognitive actions in animal models [27]. To characterize the *in vitro* anti-inflammatory effects of CMZ and NMZ, CCF-STTG1 cells were pretreated with 50 μM of CMZ or NMZ for 24 h, then treated with TNFα or LPS (1 ng/mL or 1 μg/mL, respectively) for an additional 24 h. Both agents significantly attenuated LPS-induced elevation of pro-inflammatory markers, IL-1β, TNFα, and COX2, although in TNFα-treated cells, the anti-inflammatory effects were less marked (Fig. 7A and B).

In the *ALDH2*$^{-/-}$ mTBI model, CMZ and NMZ were administered at both 20 min and 1 h post-mTBI (1 mg/kg, i.p.). NMZ significantly alleviated cognitive deficits at both time points (Fig. 7C), while CMZ only ameliorated effects when administered 20 min post-mTBI. Thus, the 20 min treatment post-mTBI was selected for further study. In the ipsilateral hemisphere of mice 24 h post-mTBI, CMZ and NMZ were able to significantly lower TNFα levels (*ALDH2*$^{-/-}$ + mTBI: 8.6 ± 2.2, *ALDH2*$^{-/-}$ + mTBI + CMZ: 3.2 ± 0.9, *ALDH2*$^{-/-}$ + mTBI + NMZ: 2.1 ± 0.6, Fig. 7D). Moreover, IL-1β levels were decreased (*ALDH2*$^{-/-}$ + mTBI: 2.7 ± 0.1, *ALDH2*$^{-/-}$ + mTBI + CMZ: 1.4 ± 0.2, *ALDH2*$^{-/-}$ + mTBI + NMZ: 1.2 ± 0.1) while COX2 remained unchanged. Several key CREB-target intermediate early genes were examined: WT and *ALDH2*$^{-/-}$ mice post-mTBI had no difference in *NRF2*, *cFOS* or *NURR1* expression (Fig. 7E), whereas with CMZ and NMZ treatment, *NRF2* levels were significantly increased (*ALDH2*$^{-/-}$ + mTBI: 1.2 ± 0.2, *ALDH2*$^{-/-}$ + mTBI + CMZ: 5.4 ± 1.3, *ALDH2*$^{-/-}$ + mTBI + NMZ: 7.6 ± 2.0). Moreover, *cFOS* and *NURR1* levels were significantly increased by NMZ (cFOS: *ALDH2*$^{-/-}$ + mTBI: 0.6 ± 0.1, *ALDH2*$^{-/-}$ + mTBI + CMZ: 1.0 ± 0.3, *ALDH2*$^{-/-}$ + mTBI + NMZ: 1.62 ± 0.17; *NURR1*: *ALDH2*$^{-/-}$ + mTBI: 1.13 ± 0.31, *ALDH2*$^{-/-}$ + mTBI + CMZ: 2.2 ± 0.4, *ALDH2*$^{-/-}$ + mTBI + NMZ: 3.6 ± 0.7). In the NOR task, daily treatment of NMZ produced a sustained rescue of cognition in NOR performance; moreover, the inflammatory suppression was sustained throughout 1 week with daily NMZ treatment (Supplemental Fig. S10).

Given the ability of NMZ to protect *ALDH2*$^{-/-}$ mice from cognitive deficits after mTBI, NMZ was explored as a procognitive agent in older mice. *ALDH2*$^{-/-}$ mice (9 months of age) were tested in the Barnes maze and NOR tasks, with administration of NMZ (1 mg/kg i.p.) 20 min prior to training. Performance in the Barnes maze and NOR tasks improved after NMZ treatment, reaching significance in NOR (Fig. 7F and G, respectively). After allowing 3 days for drug washout, the effect of NMZ in the NOR was lost. Taken together with the observations on treatment with HH and anti-amnestic agents, the behavioral deficit in *ALDH2*$^{-/-}$ mice is mild and readily, although transiently reversible.

4. Discussion

Preclinical animal models of human disease play an essential role in drug discovery. There is substantial variability amongst individuals in progression of sporadic diseases, such as ADRD. Equally, in neurotrauma, such as stroke and TBI, there is individual variability in secondary sequelae that determines the functional response after trauma. This presents a dilemma for development of preclinical models that must demonstrate statistical significance with reasonable sample size, and usually leads to the forfeit of the heterogeneity observed in human patient populations in exchange for a genetically driven homogeneity in the animal model.

The “Asian allele”, a loss-of-function mutation in *ALDH2,* prevalent in the East Asian population, has been proposed to contribute to AD risk in the general and *APOE4* carrier populations [29–31,33]. Indeed, in transgenic mice carrying the *ALDH2* mutation, 20% of 1 year old mice were reported to show signs of neurodegeneration [34]. Loss of function in mitochondrial Aldh2 reduces the capacity of mitochondria and cells to detoxify reactive aldehyde LPPs, such as HNE. Building on recent observations of a cognitive deficit observed in *ALDH2*$^{-/-}$ mice [27,28], we hypothesized that these mice would manifest a background of LPP-driven oxidative stress that would exacerbate mild neurotrauma. Both oxidative stress and mild neurotrauma contribute to risk of ADRD [9–11,13–15,74] and likely also contribute to the age-related loss of neural reserve that interacts with hallmark AD pathology to cause progression to dementia [7]. Therefore, as a foundation for this approach, we chose to study mTBI, a relatively common and mild neurotrauma, in *ALDH2*$^{-/-}$ mice.

An early event in progression of neurodegenerative disease is elevated oxidative stress accompanied by increased levels of LPP, specifically HNE, that can form neurotoxic protein and DNA adducts. In the present study, *in vitro* assays provided support for LPP and oxidative stress-mediated neuronal damage reflected by proportional increases in neuronal cell death, elevated pro-inflammatory cytokines, and activation of cell stress-response pathways, including Nrf2, with increasing concentrations of LPP (HNE and ONE). In *ALDH2*$^{-/-}$ mice, elevated HNE adducts were observed, accompanied by decreased mitochondrial function but without neuronal loss. This suggests that key mediators of mitochondrial health are impaired in *ALDH2*$^{-/-}$ mice, supporting previous findings that LPP contribute to mitochondrial dysfunction [48,75]. LPP may strongly alter normal functioning of cortical processes. The cognitive impairment in *ALDH2*$^{-/-}$ mice, significant from 4 months of age was compatible with the observed reductions in synaptic proteins, important in learning and memory in the hippocampus. However, there was no significant further decline in cognitive function in *ALDH2*$^{-/-}$ mice from 4 months to 14 months of age, and at 9 months, the cognitive deficit was readily reversed by acute administration of pro-cognitive, anti-amnestic agents. *In vitro* observations indicate a cellular stress-response to LPP that protects against higher concentrations of HNE. Similarly, in *ALDH2*$^{-/-}$ mice, there is no neuronal loss or cognitive decline with age from 4 months to 14 months, suggesting that compensatory mechanisms restrict the effects of LPP elevation to mild cognitive and synaptic dysfunction. The differential proteomic analysis was in agreement with this assessment; although highlighting some interesting changes in expression of relevant proteins, no extensive changes in protein expression were observed in cortex and hippocampus of *ALDH2*$^{-/-}$ mice compared to WT counterparts.

The effects of elevated LPP *in vitro* were exacerbated by a “2nd hit”, such as LPS and ROS (from Fe-Asc), providing support for a secondary neuronal insult against the background of elevated LPP, leading to attenuated neural reserve. In the context of this work, the lowered neural reserve was reflected by the loss of cognitive function and concommitant increase in proinflammatory biomarkers with progressive neuropathology. The effects of LPP on administration of LPS to cell lines modeling neurons and astrocytes were also reflected *in vivo*. Administration of LPS to *ALDH2*$^{-/-}$ mice and WT littermates caused the anticipated increase in pro-inflammatory biomarkers, which was significantly amplified in *ALDH2*$^{-/-}$ relative to WT mice. LPS caused significant increases in GFAP and neuronal loss in the cortex of *ALDH2*$^{-/-}$ mice relative to WT controls.

Chronic oxidative stress has been shown to exacerbate the neuropathological damage induced by TBI. The closed-skull, weight-drop model of mTBI, used as a 2nd hit in our studies, did not elicit significant or persistent effects in WT mice. In contrast, significant effects were observed in *ALDH2*$^{-/-}$ mice. These effects were most marked in the

persistence of cognitive deficits and neuroinflammation, which are components of post-concussive syndrome. Brain and plasma pro-inflammatory cytokines were significantly elevated in *ALDH2*$^{-/-}$ relative to WT mice after mTBI. Moreover GFAP, a biomarker for clinical TBI [66,76], and its proteolytic degradation products (GFAP-BDP) were significantly elevated after mTBI in *ALDH2*$^{-/-}$ mice, but not in WT controls.

Both *in vitro* and *in vivo,* the administration of known LPP scavengers attenuated the phenotype caused by elevated LPP. Neuronal loss was prevented by LPP scavengers *in vitro* and cognitive function was restored by an LPP scavenger *in vivo*, further strengthening the link between increased levels of LPP and degradation of neural reserve.

The “2-hit” model of mTBI against a background of LPP-driven oxidative stress in *ALDH2*$^{-/-}$ mice revealed dynamic behavioral and pathological changes not seen in WT controls. Moreover, in contrast to some mTBI models, the *ALDH2*$^{-/-}$ mice displayed a significant inflammatory response that is hypothesized to drive the secondary cascade following TBI. To explore the utility of this model for preclinical testing of therapeutic agents able to mitigate the effects of neurotrauma and oxidative stress, we tested two related agents, CMZ and NMZ. CMZ is a non-benzodiazepine $GABA_A$ receptor potentiator and anticonvulsant used clinically for treatment of disorders including epilepsy and anxiety in the elderly []. CMZ, under the brand name Zendra, was extensively studied as a neuroprotective agent in Phase 3 clinical trials for ischemic stroke [73,80–82,84] and continues to be recommended as a potential component of combination therapies for stroke [85]. CMZ attenuates glutamate-induced excitotoxicity and neuronal loss [86,87]. Importantly, CMZ has been shown to attenuate increases in pro-inflammatory cytokines, including TNFα, in animal models [88]. CMZ and NMZ were selected for testing. NMZ is structurally related to CMZ, retaining $GABA_A$ potentiating and anti-neuroinflammatory properties, and shown to be effective in models of ADRD, through the additional ability to activate NO/cGMP signaling and CREB [41,89–91]. Administration of both agents post-mTBI attenuated the pro-inflammatory response and cognitive deficits. Somewhat unexpectedly, both agents also significantly increased *NRF2* mRNA, suggesting that the *ALDH2*$^{-/-}$ mouse model may reveal novel mechanisms for known neuroprotective agents.

The *ALDH2*$^{-/-}$ mouse manifests mild cognitive impairment caused by LPP-induced oxidative stress resulting in synaptic dysfunction. The phenotype is readily reversed by acute treatment with a known LPP scavenger or anti-amnestic agents. The basal oxidative stress in young *ALDH2*$^{-/-}$ mice is sufficient to amplify the response to mTBI, causing significant and persistent changes relative to WT controls, most notably in pro-inflammatory biomarkers. Equally, an inflammatory insult in *ALDH2*$^{-/-}$ mice was amplified relative to WT controls and led to neuronal loss in the cortex of *ALDH2*$^{-/-}$ mice.

This new “2-hit” animal model of underlying oxidative stress with mTBI is an important addition to the small number of TBI preclinical models of mild neurotrauma. Equally, models of diminished neural resilience, a primary driver of dementia in ADRD, are urgently needed. The interaction of oxidative stress and neurotrauma in *ALDH2*$^{-/-}$ mice provides a model to explore mechanisms of loss of neural reserve and cognitive resilience, and provides a tractable preclinical model for testing novel therapeutic agents.

Funding

The work was supported by the National Institute of Aging through Grant 1T32AG057468-01 and the National Center for Advancing Translational Sciences, National Institutes of Health, through Grant UL1TR002003.

Declaration of competing interest

The authors declare that there is no conflict of interest.

Correspondence and requests for materials should be addressed to G.R.J.T (thatcher@uic.edu).

Appendix A. Supplementary data

Supplementary data to this article can be found online at https://doi.org/10.1016/j.redox.2020.101486.

References

[1] J.L. Cummings, T. Morstorf, K. Zhong, Alzheimer's disease drug-development pipeline: few candidates, frequent failures, Alzheimer's Res. Ther. 6 (4) (2014) 37.
[2] J.A. Schneider, W.Z.D.A. ArvanitakisFau - BangBang, W.D.A. Fau - BennettBennett, Mixed Brain Pathologies Account for Most Dementia Cases in Community-Dwelling Older Persons, Neurology 69 (24) (2007) 2197–2204.
[3] X. Zhu, A.K. Raina, G. Perry, M.A. Smith, Alzheimer's disease: the two-hit hypothesis, Lancet Neurol. 3 (4) (2004) 219–226.
[4] S. Chakrabarti, V.K. Khemka, A. Banerjee, G. Chatterjee, A. Ganguly, A. Biswas, Metabolic risk factors of sporadic alzheimer's disease: implications in the pathology, pathogenesis and treatment, Aging Dis. 6 (4) (2015) 282–299.
[5] K. Uryu, H. Laurer, T. McIntosh, D. Pratico, D. Martinez, S. Leight, V.M. Lee, J.Q. Trojanowski, Repetitive mild brain trauma accelerates Abeta deposition, lipid peroxidation, and cognitive impairment in a transgenic mouse model of Alzheimer amyloidosis, J. Neurosci. 22 (2) (2002) 446–454.
[6] S.J. Webster, L.J. Van Eldik, D.M. Watterson, A.D. Bachstetter, Closed head injury in an age-related Alzheimer mouse model leads to an altered neuroinflammatory response and persistent cognitive impairment, J. Neurosci. 35 (16) (2015) 6554–6569.
[7] D.A. Bennett, Mixed pathologies and neural reserve: implications of complexity for Alzheimer disease drug discovery, PLoS Med. 14 (3) (2017) e1002256.
[8] Y. Stern, Cognitive reserve, Neuropsychologia 47 (10) (2009) 2015–2028.
[9] P. Morel, C. Tallineau, R. Pontcharraud, A. Piriou, F. Huguet, Effects of 4-hydroxynonenal, a lipid peroxidation product, on dopamine transport and Na+/K+ ATPase in rat striatal synaptosomes, Neurochem. Int. 33 (6) (1998) 531–540.
[10] D.A. Butterfield, T. Reed, M. Perluigi, C. De Marco, R. Coccia, C. Cini, R. Sultana, Elevated protein-bound levels of the lipid peroxidation product, 4-hydroxy-2-nonenal, in brain from persons with mild cognitive impairment, Neurosci. Lett. 397 (3) (2006) 170–173.
[11] R.J. Mark, M.A. Lovell, W.R. Markesbery, K. Uchida, M.P. Mattson, A role for 4-hydroxynonenal, an aldehydic product of lipid peroxidation, in disruption of ion homeostasis and neuronal death induced by amyloid beta-peptide, J. Neurochem. 68 (1) (1997) 255–264.
[12] J.E. Cebak, I.N. Singh, R.L. Hill, J.A. Wang, E.D. Hall, Phenelzine protects brain mitochondrial function in vitro and in vivo following traumatic brain injury by scavenging the reactive carbonyls 4-hydroxynonenal and acrolein leading to cortical histological neuroprotection, J. Neurotrauma 34 (7) (2017) 1302–1317.
[13] R. Shringarpure, T Grune, N Sitte, K.J.A. Davies, 4-Hydroxynonenal-modified Amyloid-Beta Peptide Inhibits the Proteasome: Possible Importance in Alzheimer’s Disease, Cell Mol Life Sci 57 (12) (2000) 1802–1809.
[14] D. Pratico, S. Sung, Lipid peroxidation and oxidative imbalance: early functional events in Alzheimer's disease, J. Alzheimers Dis. 6 (2) (2004) 171–175.
[15] A. Nunomura, G. Perry, G. Aliev, K. Hirai, A. Takeda, E.K. Balraj, P.K. Jones, H. Ghanbari, T. Wataya, S. Shimohama, S. Chiba, C.S. Atwood, R.B. Petersen, M.A. Smith, Oxidative damage is the earliest event in Alzheimer disease, J. Neuropathol. Exp. Neurol. 60 (8) (2001) 759–767.
[16] E.D. Hall, R.A. Vaishnav, A.G. Mustafa, Antioxidant therapies for traumatic brain injury, Neurotherapeutics 7 (1) (2010) 51–61.
[17] C. Shao, K.N. Roberts, W.R. Markesbery, S.W. Scheff, M.A. Lovell, Oxidative stress in head trauma in aging, Free Radic. Biol. Med. 41 (1) (2006) 77–85.
[18] S. Pizzimenti, E. Ciamporcero, M. Daga, P. Pettazzoni, A. Arcaro, G. Cetrangolo, R. Minelli, C. Dianzani, A. Lepore, F. Gentile, G. Barrera, Interaction of aldehydes derived from lipid peroxidation and membrane proteins, Front. Physiol. 4 (2013) 242.
[19] T.-g. Nam, Lipid peroxidation and its toxicological implications, Toxicol. Res. 27 (1) (2011) 1–6.
[20] L. Lorente, M.M. Martin, P. Abreu-Gonzalez, L. Ramos, M. Argueso, J.J. Caceres, J. Sole-Violan, J.M. Lorenzo, I. Molina, A. Jimenez, Association between serum malondialdehyde levels and mortality in patients with severe brain trauma injury, J. Neurotrauma 32 (1) (2015) 1–6.
[21] L. Cristofori, B. Tavazzi, R. Gambin, R. Vagnozzi, C. Vivenza, A.M. Amorini, D. Di Pierro, G. Fazzina, G. Lazzarino, Early onset of lipid peroxidation after human traumatic brain injury: a fatal limitation for the free radical scavenger pharmacological therapy? J. Invest. Med. 49 (5) (2001) 450–458.
[22] F. Al Nimer, M. Strom, R. Lindblom, S. Aeinehband, B.M. Bellander, J.R. Nyengaard, O. Lidman, F. Piehl, Naturally occurring variation in the Glutathione-S-Transferase 4 gene determines neurodegeneration after traumatic brain injury, Antioxidants Redox Signal. 18 (7) (2013) 784–794.
[23] W.R. Markesbery, R.J. Kryscio, M.A. Lovell, J.D. Morrow, Lipid peroxidation is an early event in the brain in amnestic mild cognitive impairment, Ann. Neurol. 58 (5) (2005) 730–735.
[24] T.T. Reed, W.M. Pierce, W.R. Markesbery, D.A. Butterfield, Proteomic identification of HNE-bound proteins in early Alzheimer disease: insights into the role of lipid peroxidation in the progression of AD, Brain Res. 1274 (2009) 66–76.

[25] T. Reed, M. Perluigi, R. Sultana, W.M. Pierce, J.B. Klein, D.M. Turner, R. Coccia, W.R. Markesbery, D.A. Butterfield, Redox proteomic identification of 4-hydroxy-2-nonenal-modified brain proteins in amnestic mild cognitive impairment: insight into the role of lipid peroxidation in the progression and pathogenesis of Alzheimer's disease, Neurobiol. Dis. 30 (1) (2008) 107–120.
[26] K. Kitagawa, T. Kawamoto, N. Kunugita, T. Tsukiyama, K. Okamoto, A. Yoshida, K. Nakayama, Aldehyde dehydrogenase (ALDH) 2 associates with oxidation of methoxyacetaldehyde; in vitro analysis with liver subcellular fraction derived from human and Aldh2 gene targeting mouse, FEBS Lett. 476 (3) (2000) 306–311.
[27] J. Luo, S.H. Lee, L. VandeVrede, Z. Qin, M. Ben Aissa, J. Larson, A.F. Teich, O. Arancio, Y. D'Souza, A. Elharram, K. Koster, L.M. Tai, M.J. LaDu, B.M. Bennett, G.R. Thatcher, A multifunctional therapeutic approach to disease modification in multiple familial mouse models and a novel sporadic model of Alzheimer's disease, Mol. Neurodegener. 11 (1) (2016) 35.
[28] Y. D'Souza, A. Elharram, R. Soon-Shiong, R.D. Andrew, B.M. Bennett, Characterization of Aldh2 (-/-) mice as an age-related model of cognitive impairment and Alzheimer's disease, Mol. Brain 8 (1) (2015) 27.
[29] S. Ohta, I. Ohsawa, Dysfunction of mitochondria and oxidative stress in the pathogenesis of Alzheimer's disease: on defects in the cytochrome c oxidase complex and aldehyde detoxification, J. Alzheimers Dis. 9 (2) (2006) 155–166.
[30] S. Ohta, I. Ohsawa, K. Kamino, F. Ando, H. Shimokata, Mitochondrial ALDH2 deficiency as an oxidative stress, Ann. N. Y. Acad. Sci. 1011 (2004) 36–44.
[31] K. Kamino, K. Nagasaka, M. Imagawa, H. Yamamoto, H. Yoneda, A. Ueki, S. Kitamura, K. Namekata, T. Miki, S. Ohta, Deficiency in mitochondrial aldehyde dehydrogenase increases the risk for late-onset alzheimer's disease in the Japanese population, Biochem. Biophys. Res. Commun. 273 (1) (2000) 192–196.
[32] R.-L. Yu, C.-H. Tan, Y.-C. Lu, R.-M. Wu, Aldehyde dehydrogenase 2 is associated with cognitive functions in patients with Parkinson's disease, Sci. Rep. 6 (2016) 30424.
[33] S. Ohta, I. Ohsawa, Dysfunction of Mitochondria and Oxidative Stress in the Pathogenesis of Alzheimer's Disease: on Defects in the Cytochrome C Oxidase Complex and Aldehyde Detoxification, J Alzheimers Dis 9 (2) (2006) 155–166.
[34] I. Ohsawa, K. Nishimaki, Y. Murakami, Y. Suzuki, M. Ishikawa, S. Ohta, Age-dependent neurodegeneration accompanying memory loss in transgenic mice defective in mitochondrial aldehyde dehydrogenase 2 activity, J. Neurosci. 28 (24) (2008) 6239–6249.
[35] M.C.-Y. Wey, E. Fernandez, P.A. Martinez, P. Sullivan, D.S. Goldstein, R. Strong, Neurodegeneration and motor dysfunction in mice lacking cytosolic and mitochondrial aldehyde dehydrogenases: implications for Parkinson's disease, PloS One 7 (2) (2012) e31522.
[36] M. Ohta, Y. Higashi, T. Yawata, M. Kitahara, A. Nobumoto, E. Ishida, M. Tsuda, Y. Fujimoto, K. Shimizu, Attenuation of axonal injury and oxidative stress by edaravone protects against cognitive impairments after traumatic brain injury, Brain Res. 1490 (2013) 184–192.
[37] M.A. Ansari, K.N. Roberts, S.W. Scheff, Oxidative stress and modification of synaptic proteins in hippocampus after traumatic brain injury, Free Radic. Biol. Med. 45 (4) (2008) 443–452.
[38] A.G. Mustafa, I.N. Singh, J. Wang, K.M. Carrico, E.D. Hall, Mitochondrial protection after traumatic brain injury by scavenging lipid peroxyl radicals, J. Neurochem. 114 (1) (2010) 271–280.
[39] B.M. Bennett, J.N. Reynolds, G.T. Prusky, R.M. Douglas, R.J. Sutherland, G.R.J. Thatcher, Cognitive deficits in rats after forebrain cholinergic depletion are reversed by a novel NO mimetic nitrate ester, Neuropsychopharmacology 32 (3) (2007) 505–513.
[40] S.C. Tang, T.V. Arumugam, R.G. Cutler, D.G. Jo, T. Magnus, S.L. Chan, M.R. Mughal, R.S. Telljohann, M. Nassar, X. Ouyang, A. Calderan, P. Ruzza, A. Guiotto, M.P. Mattson, Neuroprotective actions of a histidine analogue in models of ischemic stroke, J. Neurochem. 101 (3) (2007) 729–736.
[41] J. Luo, S.H. Lee, L. VandeVrede, Z. Qin, S. Piyankarage, E. Tavassoli, R.T. Asghodom, M. Ben Aissa, M. Fa, O. Arancio, L. Yue, D.R. Pepperberg, G.R. Thatcher, Re-engineering a neuroprotective, clinical drug as a procognitive agent with high in vivo potency and with GABAA potentiating activity for use in dementia, BMC Neurosci. 16 (2015) 67.
[42] S. Lorrio, P. Negredo, J.M. Roda, A.G. Garcia, M.G. Lopez, Effects of memantine and galantamine given separately or in association, on memory and hippocampal neuronal loss after transient global cerebral ischemia in gerbils, Brain Res. 1254 (2009) 128–137.
[43] A.V. Terry Jr., P.M. Callahan, B. Hall, S.J. Webster, Alzheimer's disease and age-related memory decline (preclinical), Pharmacol. Biochem. Behav. 99 (2) (2011) 190–210.
[44] M. Leger, A. Quiedeville, V. Bouet, B. Haelewyn, M. Boulouard, P. Schumann-Bard, T. Freret, Object recognition test in mice, Nat. Protoc. 8 (12) (2013) 2531–2537.
[45] R.M. Deacon, Assessing nest building in mice, Nat. Protoc. 1 (3) (2006) 1117–1119.
[46] O. Zohar, S. Schreiber, V. Getslev, J.P. Schwartz, P.G. Mullins, C.G. Pick, Closed-head minimal traumatic brain injury produces long-term cognitive deficits in mice, Neuroscience 118 (4) (2003) 949–955.
[47] N. Rauniyar, J.R. Yates 3rd, Isobaric labeling-based relative quantification in shotgun proteomics, J. Proteome Res. 13 (12) (2014) 5293–5309.
[48] S.O. Abarikwu, A.B. Pant, E.O. Farombi, 4-Hydroxynonenal induces mitochondrial-mediated apoptosis and oxidative stress in SH-SY5Y human neuronal cells, Basic Clin. Pharmacol. Toxicol. 110 (5) (2012) 441–448.
[49] C. Werner, K. Engelhard, Pathophysiology of traumatic brain injury, Br. J. Anaesth. 99 (1) (2007) 4–9.
[50] A Guiotto, A Calderan, P Ruzza, A Osler, C Rubini, DG Jo, MP Mattson, G Borin, Synthesis and Evaluation of Neuroprotective Alpha,beta-Unsaturated Aldehyde Scavenger Histidyl-Containing Analogues of Carnosine, J Med Chem 48 (19) (2005) 6156–6161.
[51] S.C. Tang, V. Arumugam Thiruma, G. Cutler Roy, D.G. Jo, T. Magnus, L. Chan Sic, R. Mughal Mohamed, S. Telljohann Richard, M. Nassar, X. Ouyang, A. Calderan, P. Ruzza, A. Guiotto, P. Mattson Mark, Neuroprotective actions of a histidine analogue in models of ischemic stroke, J. Neurochem. 101 (3) (2006) 729–736.
[52] G Olivieri, G Baysang, F Meier, F Müller-Spahn, HB Stähelin, M Brockhaus, C Brack, N-acetyl-L-cysteine Protects SHSY5Y Neuroblastoma Cells from Oxidative Stress and Cell Cytotoxicity: Effects on Beta-Amyloid Secretion and Tau Phosphorylation, J Neurochem 76 (1) (2001) 224–233.
[53] R. Bavarsad Shahripour, M.R. Harrigan, A.V. Alexandrov, N-acetylcysteine (NAC) in neurological disorders: mechanisms of action and therapeutic opportunities, Brain and Behav 4 (2) (2014) 108–122.
[57] A.K. Kraeuter, P.C. Guest, Z. Sarnyai, The Y-maze for assessment of spatial working and reference memory in mice, Methods Mol. Biol. 1916 (2019) 105–111.
[58] S.S. Patil, B. Sunyer, H. Hoger, G. Lubec, Evaluation of spatial memory of C57BL/6J and CD1 mice in the Barnes maze, the Multiple T-maze and in the Morris water maze, Behav. Brain Res. 198 (1) (2009) 58–68.
[59] C.S. Rosenfeld, S.A. Ferguson, Barnes maze testing strategies with small and large rodent models, J. Vis. Exp. 84 (2014) e51194.
[60] J.B. Melo, C. Sousa, P. Garcao, C.R. Oliveira, P. Agostinho, Galantamine protects against oxidative stress induced by amyloid-beta peptide in cortical neurons, Eur. J. Neurosci. 29 (3) (2009) 455–464.
[61] C. Pieta Dias, M.N. Martins de Lima, J. Presti-Torres, A. Dornelles, V.A. Garcia, F. Siciliani Scalco, M. Rewsaat Guimaraes, L. Constantino, P. Budni, F. Dal-Pizzol, N. Schroder, Memantine reduces oxidative damage and enhances long-term recognition memory in aged rats, Neuroscience 146 (4) (2007) 1719–1725.
[62] Y.W. Kim, T.V. Byzova, Oxidative stress in angiogenesis and vascular disease, Blood 123 (5) (2014) 625–631.
[63] S. Page, C. Fischer, B. Baumgartner, M. Haas, U. Kreusel, G. Loidl, M. Hayn, H.W. Ziegler-Heitbrock, D. Neumeier, K. Brand, 4-Hydroxynonenal prevents NF-kappaB activation and tumor necrosis factor expression by inhibiting IkappaB phosphorylation and subsequent proteolysis, J. Biol. Chem. 274 (17) (1999) 11611–11618.
[64] N.A. Essani, M.A. Fisher, H. Jaeschke, Inhibition of NF-kappa B activation by dimethyl sulfoxide correlates with suppression of TNF-alpha formation, reduced ICAM-1 gene transcription, and protection against endotoxin-induced liver injury, Shock 7 (2) (1997) 90–96.
[65] E. Mariani, M.C. Polidori, A. Cherubini, P. Mecocci, Oxidative stress in brain aging, neurodegenerative and vascular diseases: an overview, J. Chromatogr. B Analyt Technol. Biomed. Life Sci. 827 (1) (2005) 65–75.
[66] D.O. Okonkwo, J.K. Yue, A.M. Puccio, D.M. Panczykowski, T. Inoue, P.J. McMahon, M.D. Sorani, E.L. Yuh, H.F. Lingsma, A.I. Maas, A.B. Valadka, G.T. Manley, R. Transforming, I. Clinical Knowledge in Traumatic Brain Injury, GFAP-BDP as an acute diagnostic marker in traumatic brain injury: results from the prospective transforming research and clinical knowledge in traumatic brain injury study, J. Neurotrauma 30 (17) (2013) 1490–1497.
[67] J. Lei, G. Gao, J. Feng, Y. Jin, C. Wang, Q. Mao, J. Jiang, Glial fibrillary acidic protein as a biomarker in severe traumatic brain injury patients: a prospective cohort study, Crit. Care 19 (2015) 362.
[68] T.M. Luoto, R. Raj, J.P. Posti, A.J. Gardner, W.J. Panenka, G.L. Iverson, A systematic review of the usefulness of glial fibrillary acidic protein for predicting acute intracranial lesions following head trauma, Front. Neurol. 8 (2017) s.
[69] Z. Zhang, J.S. Zoltewicz, S. Mondello, K.J. Newsom, Z. Yang, B. Yang, F. Kobeissy, J. Guingab, O. Glushakova, S. Robicsek, S. Heaton, A. Buki, J. Hannay, M.S. Gold, R. Rubenstein, X.C. Lu, J.R. Dave, K. Schmid, F. Tortella, C.S. Robertson, K.K. Wang, Human traumatic brain injury induces autoantibody response against glial fibrillary acidic protein and its breakdown products, PloS One 9 (3) (2014) e92698.
[70] L. Wang, K.J. Colodner, M.B. Feany, Protein misfolding and oxidative stress promote glial-mediated neurodegeneration in an Alexander disease model, J. Neurosci. 31 (8) (2011) 2868–2877.
[71] M.V. Patel, E. Sewell, S. Dickson, H. Kim, D.F. Meaney, B.L. Firestein, A role for postsynaptic density 95 and its binding partners in models of traumatic brain injury, J. Neurotrauma 36 (13) (2019) 2129–2138.
[72] C. Wakade, S. Sukumari-Ramesh, M.D. Laird, K.M. Dhandapani, J.R. Vender, Delayed reduction in hippocampal postsynaptic density protein-95 expression temporally correlates with cognitive dysfunction following controlled cortical impact in mice, J. Neurosurg. 113 (6) (2010) 1195–1201.
[73] A.R. Green, Clomethiazole (Zendra) in acute ischemic stroke: basic pharmacology and biochemistry and clinical efficacy, Pharmacol. Ther. 80 (2) (1998) 123–147.
[74] P. Jenner, Oxidative stress in Parkinson's disease, Ann. Neurol. 53 (Suppl 3) (2003) S36–S38.
[75] M. Dodson, W.Y. Wani, M. Redmann, G.A. Benavides, M.S. Johnson, X. Ouyang, S.S. Cofield, K. Mitra, V. Darley-Usmar, J. Zhang, Regulation of autophagy, mitochondrial dynamics, and cellular bioenergetics by 4-hydroxynonenal in primary neurons, Autophagy 13 (11) (2017) 1828–1840.
[76] P.E. Vos, B. Jacobs, T.M. Andriessen, K.J. Lamers, G.F. Borm, T. Beems, M. Edwards, C.F. Rosmalen, J.L. Vissers, GFAP and S100B are biomarkers of traumatic brain injury: an observational cohort study, Neurology 75 (20) (2010) 1786–1793.
[80] J.W. Marshall, A.J. Cross, R.M. Ridley, Functional benefit from clomethiazole treatment after focal cerebral ischemia in a nonhuman primate species, Exp. Neurol. 156 (1) (1999) 121–129.
[81] M. Farooque, J. Isaksson, D.M. Jackson, Y. Olsson, Clomethiazole (ZENDRA, CMZ) improves hind limb motor function and reduces neuronal damage after severe spinal cord injury in rat, Acta Neuropathol (Berl) 98 (1) (1999) 22–30.
[82] N.G. Wahlgren, E. Diez-Tejedor, J. Teitelbaum, A. Arboix, D. Leys, T. Ashwood, E. Grossman, Results in 95 hemorrhagic stroke patients included in CLASS, a

controlled trial of clomethiazole versus placebo in acute stroke patients, Stroke 31 (1) (2000) 82–85.
[84] P. Lyden, A. Shuaib, K. Ng, K. Levin, R.P. Atkinson, A. Rajput, L. Wechsler, T. Ashwood, L. Claesson, T. Odergren, E. Salazar-Grueso, Clomethiazole Acute Stroke Study in ischemic stroke (CLASS-I): final results, Stroke 33 (1) (2002) 122–128.
[85] M.J. Wilby, P.J. Hutchinson, The pharmacology of chlormethiazole: a potential neuroprotective agent? CNS Drug Rev. 10 (4) (2004) 281–294.
[86] D. Harmon, E. Coleman, C. Marshall, W. Lan, G. Shorten, The effect of clomethiazole on plasma concentrations of interleukin-6, -8, -1beta, tumor necrosis factor-alpha, and neutrophil adhesion molecule expression during experimental extracorporeal circulation, Anesth. Analg. 97 (1) (2003) 13–18.
[87] A.N. Clarkson, H. Liu, R. Rahman, D.M. Jackson, I. Appleton, D.S. Kerr, Clomethiazole: mechanisms underlying lasting neuroprotection following hypoxia-ischemia, Faseb. J. 19 (8) (2005) 1036–1038.
[88] A.N. Clarkson, J. Clarkson, D.M. Jackson, I.A. Sammut, Mitochondrial involvement in transhemispheric diaschisis following hypoxia-ischemia: clomethiazole-mediated amelioration, Neuroscience 144 (2) (2007) 547–561.
[89] L. Vandevrede, E. Tavassoli, J. Luo, Z. Qin, L. Yue, D.R. Pepperberg, G.R. Thatcher, Novel analogues of chlormethiazole are neuroprotective in four cellular models of neurodegeneration by a mechanism with variable dependence on GABA(A) receptor potentiation, Br. J. Pharmacol. 171 (2) (2014) 389–402.
[90] J. Luo, S.H. Lee, L. VandeVrede, Z. Qin, M. Ben Aissa, J. Larson, A.F. Teich, O. Arancio, Y. D'Souza, A. Elharram, K. Koster, L.M. Tai, M.J. LaDu, B.M. Bennett, G.R. Thatcher, A multifunctional therapeutic approach to disease modification in multiple familial mouse models and a novel sporadic model of Alzheimer's disease, Mol. Neurodegener. 11 (2016) 35.
[91] B.M. Bennett, J.N. Reynolds, G.T. Prusky, R.M. Douglas, R.J. Sutherland, G.R.J. Thatcher, Cognitive deficits in rats after forebrain cholinergic depletion are reversed by a novel NO mimetic nitrate ester, Neuropsychopharmacology 32 (2006) 505.
[93] C. Ceconi, S. Curello, A. Cargnoni, R. Ferrari, A. Albertini, O. Visioli, The role of glutathione status in the protection against ischaemic and reperfusion damage: effects of N-acetyl cysteine, J Mol Cell Cardiol 20 (1) (1988) 5–13.